EXPERIMENTAL AND MODELING STUDY OF GAS ADSORPTION IN METAL-ORGANIC FRAMEWORK COATED ON 3D PRINTED PLASTICS

A Thesis

Submitted to the Faculty

of

Purdue University

by

Tejesh C. Dube

In Partial Fulfillment of the

Requirements for the Degree

of

Master of Science Mechanical Engineering

May 2020

Purdue University

Indianapolis, Indiana

THE PURDUE UNIVERSITY GRADUATE SCHOOL
STATEMENT OF THESIS APPROVAL

Dr. Jing Zhang, Chair

Department of Mechanical and Energy Engineering

Dr. Andres Tovar

Department of Mechanical and Energy Engineering

Dr. Xiaoliang Wei

Department of Mechanical and Energy Engineering

Approved by:

Dr. Jie Chen

Head of the Graduate Program

To my grandmother Mrs. J. Chauhan
who dedicated her life to education

ACKNOWLEDGMENTS

I am immensely grateful to Dr.Jing Zhang for his valuable guidance, support and always motivating persona to push me through this project. I really appreciate his leadership and help for providing all the necessary resources and knowledge required for this thesis. His constant encouragement helped me work on other projects and present papers and posters at several reputed conferences.

I would also like to thank Dr. Tovar and Dr. Wei for being on my thesis committee and for being a part of this project. Thank you for your time and consideration.

I would like to thank Prof. Yeon-Gil Jung and Hye-Yeong Park for helping us with SEM and XRD analysis of all the samples.

This work is partially supported by "Human Resources Program in Energy Technology (No. 20194030202450) " and "Power Generation & Electricity Delivery grant (No. 20193310100030)" of the Korea Institute of Energy Technology Evaluation and Planning (KETEP).

I would like to thank my lab mates Swapnil, Harshal, Abhilash, Piyush, Anvesh, Xuehui, Lingbin and Jian for helping me with any problems that surfaced during this project.

Last, but not the least, my grandmother, parents, my family and my friends Sailee, Jay, Fermin and Tripthi for always standing by my side.

TABLE OF CONTENTS

Page

LIST OF TABLES

LIST OF FIGURES

Figure Page

ABSTRACT

Dube, Tejesh C., M.S.M.E., Purdue University, May 2020. Experimental and Modeling Study of Gas Adsorption in Metal-Organic Framework Coated on 3D Printed Plastics. Major Professor: Jing Zhang.

Metal-organic frameworks (MOFs) are a class of compounds consisting of metal ions or clusters coordinated to organic ligands in porous structure forms. MOFs have been proposed in use for gas adsorption, purification, and separation applications. This work combines MOFs with 3D printing technologies, in which 3D printed plastics serve as a mechanical structural support for MOFs powder, in order to realize a component design for gas adsorption. The objective of the thesis is to understand the gas adsorption behavior of MIL-101 (Cr) MOF coated on 3D printed PETG, a glycol modified version of polyethylene terephthalate, through a combined experimental and modeling study. The specific goals are: (1) synthesis of MIL-101 (Cr) MOFs; (2) nitrogen gas adsorption measurements and microstructure and phase characterization of the MOFs; (3) design and 3D printing of porous PETG substrate structures; (4) deposition of MOFs coating on the PETG substrates; and (5) Monte Carlo (MC) modeling of sorption isotherms of nitrogen and carbon dioxide in the MOFs.

The results show that pure MIL-101 (Cr) MOFs were successfully synthesized, as confirmed by the scanning electron microscopy (SEM) images and X-ray diffraction (XRD), which are consistent with literature data. The Brunauer-Emmett-Teller (BET) surface area measurement shows that the MOFs samples have a high coverage of nitrogen. The specific surface area of a typical MIL-101 (Cr) MOFs sample is 2716.83 m2/g. MIL-101 (Cr) also shows good uptake at low pressures in experimental tests for nitrogen adsorption. For the PETG substrate, disk-shape plastic samples with a controlled pore morphology were designed and fabricated using the fused de-

position modeling (FDM) process. MOFs were coated on the PETG substrates using a layer-by-layer (LbL) assembly approach, up to 30 layers. The MOFs coating layer thicknesses increase with the number of deposition layers. The computational model illustrates that the MOFs show increased outputs in adsorption of nitrogen as pressure increases, similar to the trend observed in the adsorption experiment. The model also shows promising results for carbon dioxide uptake at low pressures, and hence the developed MOFs based components would serve as a viable candidate in gas adsorption applications.

1. INTRODUCTION

Metal Organic Frameworks (MOF) form a new class of microporous crystalline structures comprising of metal ions held together by organic ligands [1].They are gaining wide popularity due to their versatile role in various applications ranging from optics, electronics and magnetism to ion exchange, chirality, adsorption and catalysis. MOFs are widely used in the field of gas purification for lowering sulfur levels. Most power plants require various gases for energy production which are stored in high pressure tanks equipped with a multistage compressor unit. This storage facility requires high maintenance and therefore adds to the expenses. The high porosity and good crystalline form of MOFs makes them a suitable candidate in gas storage applications. Recently, some of the MOFs have also been investigated in the field of biomedical applications. The study shows that MOFs can be used to carry drugs but important factors like nontoxicity and biocompatibility should be taken into consideration.

1.1 Motivation

With the rising environmental concerns due to pollution, especially the green house emissions, it has become a necessity to find a solution to this crisis. MOFs standout as promising candidates because of their highly porous structures. They are currently being used in purification and filtration applications.The metal sites present in MOFs act as attractive sites for gas molecule binding. Gas storage and transportation is another area where MOFS can venture and come out with flying colors. Their gas binding abilities could be used for storing and transporting highly reactive gases. A similar class of materials, carbon nano tubes, have shown exceptional results for storing hydrogen at low pressure and low temperature.

1.2 Objective

This work combines MOFs with 3D printing technologies, in which 3D printed plastics serve as a mechanical structural support for MOFs powder, in order to realize a component design for gas adsorption. The objective of the thesis is to understand the gas adsorption behavior of MIL-101 (Cr) MOF coated on 3D printed PETG, a glycol modified version of polyethylene terephthalate, through a combined experimental and modeling study. The specific goals are:

1. Synthesis of MIL-101 (Cr) MOFs
2. Nitrogen gas adsorption measurements and microstructure and phase characterization of the MOFs
3. Design and 3D printing of porous PETG substrate structures;
4. Deposition of MOFs coating on the PETG substrates; and
5. Monte Carlo (MC) modeling of sorption isotherms of nitrogen and carbon dioxide in the MOFs

1.3 Structure of Thesis

This work is divided into seven chapters. The first chapter deals with the basic introduction, the motivation and the objective of this study.
The second chapter reviews the literature which is relevant in understanding the basic concepts used in this work.It also sheds light on some of the ongoing research related to the objective of this study.
The third chapter covers the experimental approach incorporated in synthesizing MIL-101 (Cr) powder in-house, printing PETG substrate and developing MIL-101(Cr) coatings on the printed PETG substrates. The fourth chapter models the computational study undertaken to analyse and evaluate the performance of MOFs for adsorption of nitrogen and carbon dioxide. The fifth chapter sheds light on the results

and discusses the outcomes of the various experimental and computational tests. It also discusses the viability of the proposed approach. The sixth chapter concludes and summarizes the findings of this work and the seventh chapter showcases the contributions of this study to the existing knowledge in this field. Chapter eight looks into the future dimensions of this work and states down the plausible modifications and new findings related to this study.

2. LITERATURE REVIEW

2.1 Gas Storage

Currently, the most popular way for transporting and storing gases is by compressing them into cylinders. This poses as a viable solution for moving some highly reactive gases like hydrogen from the production facility to their target source of application. Another popular method is to transport them using high pressure pipelines. But both of these methods come with their own consequences. First and foremost problem while using these methods is the possibility of an explosion due to the gases being under high pressure in a confined space. The second is a high cost associated with manufacturing and maintaining a system that can contain and prevent any possible leakages while monitoring the physical properties of the gas. A lot of research has been done on creating risk assessment and prevention models for gas storage and transportation [2]. Researchers have also worked on developing cost effective models to lower the cost incurred in production and maintenance of equipment and facility for the same [3] [4] [5]. However, it still comes with a certain risk factor.

A novel approach has been researched recently that allows the gases to be stored at low pressures thereby almost nullifying the risk associated with its storage and transportation. Gases can be adsorbed onto the substrates at low pressures. Such a technique was used for storing natural gas on activated carbon [6]. Adsorbed natural gas (ANG) process served as a better alternative for storing natural gas as compared to Compressed natural gas (CNG) and Liquefied natural gas (LNG). In a CNG system, the natural gas is compressed to a pressure of 20 MPa for storage. To achieve this, the natural gas has to pass through a system of multistage compression at the filling stations, filled in a thick walled pressure vessel and sealed of with a high pressure safety valve. The cost associated with this system is very high and also

moving and storing natural gas at such high pressure comes with a high risk factor. In case of a LNG system, the natural gas is liquefied using expensive cryogenic systems which again impacts on the cost associated and hence affects the feasibility of the process. In the ANG system, the natural gas is adsorbed onto porous activated carbon and stored at a moderate pressure of 3.5 to 4 MPa. The ANG system has also achieved a storage target of 180 V/V (litres of gas stored per litres of storage vessel internal volume at NTP) specified by the US Department of Energy [7].

An alarming increase in the CO2 emissions in the past decades has increased the concerns over the polar caps melting and global warming along with other health hazards. The Green House Gases (GHG) emissions have increased by 41 percent since 1990 [8]. Although recently, there has been a drop in the emission volumes but still the concern remains active as the GHG's contribute to roughly 1°C increase in global temperatures since pre-industrial times [9].

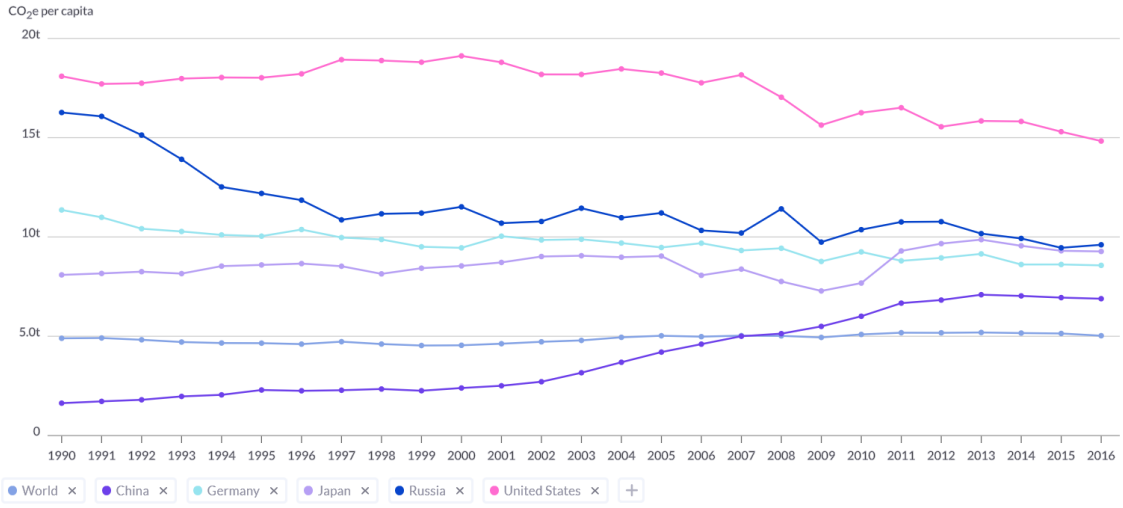

Fig. 2.1. CO_2 Emission Chart 1990-2016 [8]

Therefore the need to contain and control the GHG emissions is of utmost importance. The GHG gases mainly comprise of Carbon di Oxide (CO_2), Methane (CH_4), Nitrous oxide (N_2O) and Ozone (O_3) [9]. Most of these gases are produced as a result of combustion of fossil fuels which still serve as the major energy source.

2.2 Adsorption

Adsorption is a surface phenomenon wherein the atoms, ions or dissolved solids are adhered to a surface. The species that adheres is called adsorbate and the substrate on which the adsorbate adheres is called the adsorbent.

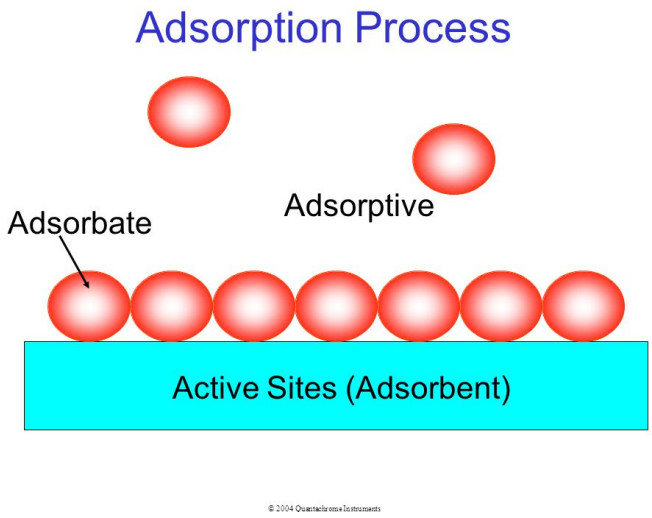

Fig. 2.2. Adsorption Phenomenon

As stated earlier, adsorption is a surface phenomenon as opposed to absorption which involves the whole volume of the material. Just like surface tension phenomenon, adsorption is also governed by surface energy. Unlike the atoms in the bulk phase, surface atoms have open valencies due to which they attract foreign species to stick to the surface and hence form a weak bond. As a result of these weak bonds adsorption is a reversible process. Adsorption can be further classified into physical and chemical adsorption based on how it occurs. In simple terms, physical adsorption (also called physisorption) does not disturb the chemical structure of an atom or molecule and occurs mostly due to van der Walls forces. Although the interaction energy is very weak (10-100 meV), physisorption plays an important role in nature. For example, van der Walls forces between the surface and gecko's foot hair give them the ability to stick to the surface and climb vertical walls. Chemical

adsorption *chemisorption*, on the other hand, is a type of adsorption in which the adsorbate and the surface atoms on the adsorbent indulge in a chemical reaction thereby modifying the chemical structure of the atom or molecule [10]. Corrosion is an example of chemisorption in which the surface atoms of the adsorbent reacts with oxygen and forms metal oxide. Chemisorption is not fully reversible due to the fact that adsorbate and adsorbent share electrons to form either covalent or ionic bonds which require high energy to cleave [11]. But most of the gases, for storage purpose, adopt physisorption phenomenon. We would be looking deeper into physisorption and its mechanism in the next section.

2.2.1 Physisorption

Physisorption occurs when the intermolecular attractive forces between the adsorbate and adsorbent is greater than the intermolecular attractive forces between adsorbate molecules [12]. The enthalpy change during physisorption is given as :

$$\Delta H = \Delta G + T\Delta S \tag{2.1}$$

The entropy change,ΔS is mostly negative for physisorption because of the fact that adsorbed state is more ordered as compared to the unadsorbed state. The change in Gibbs free energy, ΔG is also negative for a spontaneous physisorption. This results in a negative ΔH and therefore it states that physical adsorption is an *exothermic* process. An increase in adsorption in temperature then invariably results in a decrease of uptake capacity [12]

The interaction between the adsorbate and adsorbent is governed by very weak forces such as van der Walls forces, electrostatic forces due to dipole attraction or hydrogen bonds.

2.2.2 Adsorption Isotherms

Adsorption isotherms help draw a better picture of adsorption by establishing a relation between the amount of gas adsorbed and the partial pressure at a constant temperature.The quantity of gas adsorbed can be stated in any unit: grams, moles, volume (STP) per unit area or per gram of the adsorbent. The relative pressure is represented as $\frac{P}{P_0}$. Physisorption can occur at any interface: solid-liquid, liquid-gas or solid-gas. We will be particularly looking at the physiosorption occurring at solid-gas interface. Physisorption at solid-gas interface can be classified into 6 types as per figure 2.3

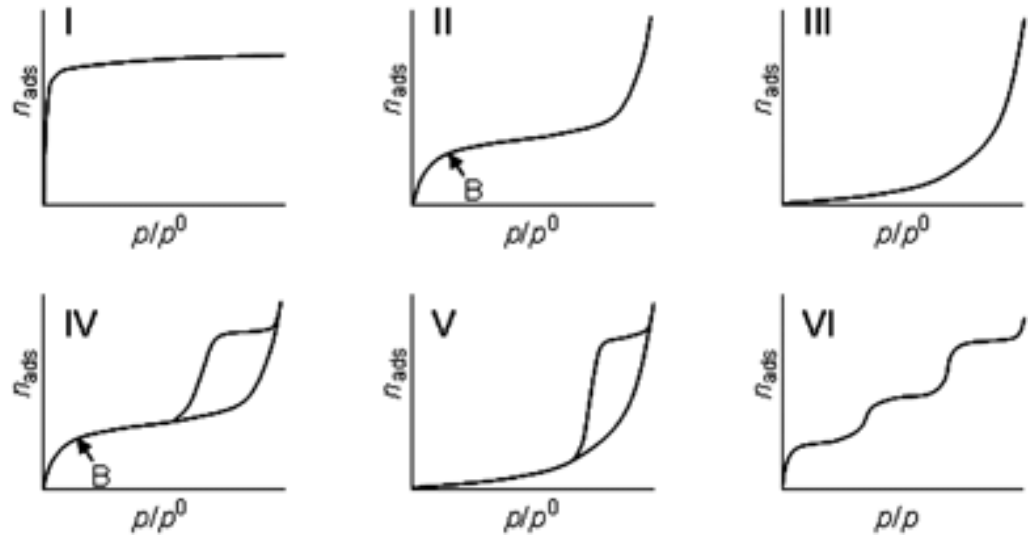

Fig. 2.3. Types of Physisorption Isotherms [13]

Type I

Type I isotherms are characteristics for microporous solids. Adsorbed gas quantity (n_{ads}) approaches a limiting value due to the lack of an external surface area. They are generally modeled using Langmuir isotherm equation.

Type II

Type II isotherms resemble type I in the initial phase. However n_{ads} does not saturate as in type I because point B marks as the start of multilayer adsorption. Once a monolayer of adsorbate has adhered to the adsorbent surface, the adsorbate-adsorbate attraction results in progressive adsorption. This is a characteristic of non-porous or macroporous solids. This type of isotherm represents reversible adsorption.

Type III

Type III is very similar to type II isotherm, only difference being a stagnated start. This isotherm is characteristic of gases which have very low affinity to the adsorbent. The initial slope is very low, but once some molecules are adsorbed, a similar phenomenon occurs as in multilayer adsorption and facilitates for further adsorption. Type III is also a reversible isotherm.

Type IV and V

Types IV and V show hystersis as 'P' approaches 'P_0'. Hystersis indicates capillary condensation. Type IV is usually associated with type II and commonly found in industrial adsorbents whereas type V is associated with type III and is not that common.

Type VI

Type VI characterizes idealized conditions for uniform non-porous solids. The steps represent adsorption at every monolayer and remains constant for 2 or 3 layers.

Adsorption isotherms not only help in understanding the physisorption but are more often used to measure the heat of desorption. The next section explains the procedure and concept behind this.

2.2.3 Brunauer-Emmett-Teller Theory

In 1938, Stephen Brunauer, Paul Hugh Emmett and Edward teller published the first article about the BET theory in the Journal of the American Chemical Society [14]. BET theory is an extension to Langmuir adsorption theory. Langmuir adsorption model just considered adsorption at monolayer whereas BET focuses on multilayer adsorption. To make it easier to apprehend, BET theory has stated some hypotheses [15] [16].

1. The gas is perfect.
2. Adsorbed molecules are classical objects localized on their adsorption sites.
3. The surface is characterized by N_m identical sites.
4. Adsorption takes place either on surface sites or on the top of molecules already adsorbed (in-between positions are excluded).
5. The first layer only interacts with the surface; all other layers have interparticle interaction with the same energy as would apply in the liquid state, and involving only nearest neighbours in the vertical stack of adsorbed atoms in each site.
6. Adsorbed molecules do not interact laterally.

Based on these hypotheses, an expression for BET theory can be stated. [17].

$$\frac{P}{V(P_0 - P)} = \frac{1}{V_m c} + (\frac{c-1}{V_m c})(\frac{P}{P_0}) \tag{2.2}$$

where,

P= Pressure applied

P_0= Vapor pressure of gas

V= Volume of adsorbed gas

V_m= Volume of gas adsorbed at monolayer

C= BET constant

The above stated equation is of the form y=mx + b where m= $(\frac{c-1}{V_m c})$ and b= $\frac{1}{V_m c}$. The BET constant, C is given as [17]:

$$C = exp^{\frac{\Delta_{des}H - \Delta_{vap}H}{R*T}} \tag{2.3}$$

where,

$\Delta_{des}H$ = Heat of desorption

$\Delta_{vap}H$ = Heat of vaporisation

R= gas constant

T= Temperature of the gas

The expression in Equation 2.2 represents a line and the linearity of the curve is only maintained in the range of $0.05 < \frac{P}{P_0} < 0.35$ [18] [19] [20] [21].The BET theory is largely used to determine specific surface area of the solid substrate. A standard procedure to do so incorporates the use of nitrogen at its boiling temperature (77 K) and measure the adsorption at first layer. We will be using BET theory in the upcoming sections to analyse specific solid surfaces.

2.3 Metal Organic Frameworks

Metal organic frameworks (MOFs) constitute another class of materials suitable for gas adsorption. This family of materials can be chemically synthesized and offer a wide variety of pore sizes thereby making their application flexible with different gases. MOFs form microporous crystalline structures comprising of metal ions held together by organic ligands [1]. They are gaining wide popularity due to their versatile role in various applications ranging from optics, electronics and magnetism to ion exchange, chirality, adsorption and catalysis [22]. MOFs are widely used in the field of gas purification for lowering sulfur levels. Most power plants require various gases for energy production which are stored in high pressure tanks equipped with a multistage compressor unit. This storage facility requires high maintenance and therefore adds

to the expenses. The high porosity and good crystalline form of MOFs makes them a suitable candidate in gas storage applications. Recently, some of the MOFs have also been investigated in the field of biomedical applications. The study shows that MOFs can be used to carry drugs but important factors like nontoxicity and biocompatibility should be taken into consideration [23]. This study involves synthesizing and evaluating MIL-101 (Cr) (Figure 2.4), a chromium based MOF for gas adsorption applications. MIL-101 (Cr) molecule comprises of Chromium (III)(Cr(III)) atoms linked together by terephthalate ligands. The adsorption of gas molecule is credited to the active metal sites of unsaturated Cr (III) capable of capturing the gas molecule by Lewis acid-base interactions between atoms of gas molecule and Cr(III). MIL-101 (Cr) has large pore size, high BET surface area and affinity to capture gas molecules which makes it a competent candidate in gas adsorption applications.

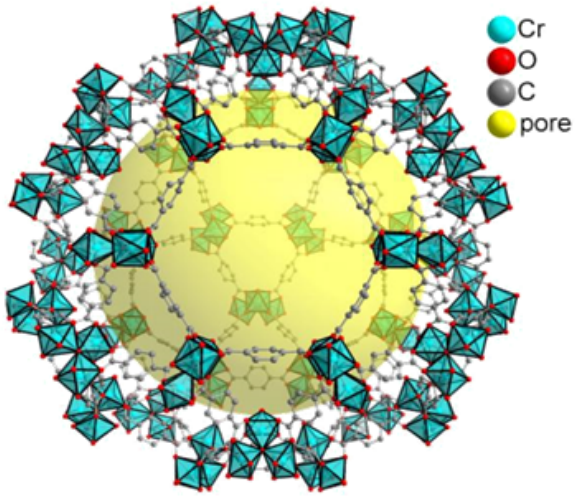

Fig. 2.4. MIL-101 (Cr) Graphical Representation [24]

Due to these properties, MOFs can be used to trap gases accounting towards pollution and thus can help in pollution control. The only drawback with them is their processability. MOFs exist in powder form and are structurally unstable. In order to make them suitable for emission control applications, they should be robust. Current coating approaches are focused on growing MOFs from the substrate

which requires elaborate surface treatments, high temperatures or the use of organic solvents [25] [26] [27] [28].However, such an approach limits the substrate choice and affects the quality of the coating [29] [30].To address this issue, a layer-by-layer (LbL) assembly approach was used. The principle of electrostatic attraction is incorporated in the LbL approach [31] [32] [33].

3. EXPERIMENTS

3.1 Synthesis of MIL-101 (Cr)

MIL-101 (Cr) was synthesized in house by following the protocol defined by a previous research [34].

Table 3.1.
Chemical composition of MIL-101 (Cr)

Chemical Used	**Quantity**
Chromium (III) Nitrate Nanohydrate	330 mg
Terephthalic Acid	136.9 mg
4-methoxy benzoic acid	5.1 mg

Chromium (III) nitrate nanohydrate (MilliporeSigma, St. Louis, MO, USA), terephthalic acid (MilliporeSigma, St. Louis, MO, USA) and 4-methoxy benzoic acid (MilliporeSigma, St. Louis, MO, USA) were added to 25 ml deionized water (DI water) (MilliporeSigma, St. Louis, MO, USA) as per the quantities specified in Table 3.1.The mixture was then sonicated at room temperature to form a homogeneous solution. It was then heated to 180°C for 4 hours in a Teflon lined autoclave. The reaction mixture was cooled down to room temperature and filtered using a $0.2\mu m$ bottle top filter to remove any unreacted terephthalic acid. A green precipitate was obtained after filtering which was washed three times with DI water and methanol (MilliporeSigma, St. Louis, MO, USA) to get pure MIL-101 (Cr) powder.

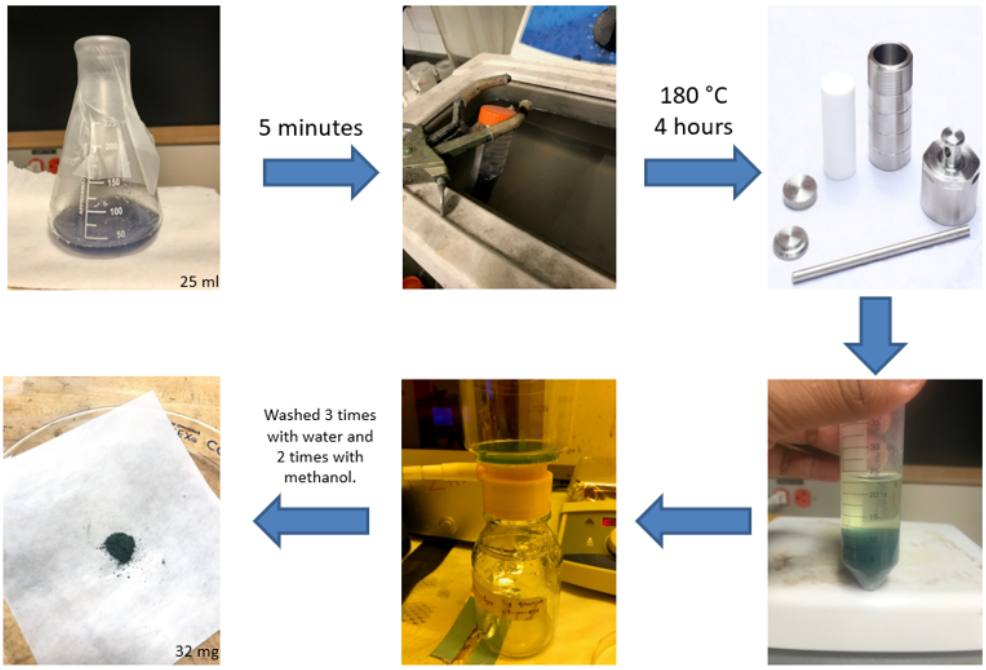

Fig. 3.1. MIL-101 (Cr) Synthesis

3.2 3D printing of PETG Substrate

Substrates were printed using Fused Deposition Melting (FDM) technique. Polyethylene Terephthalate- Glycol (PETG) (MatterHackers, Lake Forest, CA, USA) was used as the material for printing the substrates. It was selected based on its success stated in a previous research [35]. A sieve like geometry was developed for the substrate to enhance the part's adsorption capabilities. The CAD design (Figure 3.2) was modeled on Creo 4.0 and the substrate was printed on a MakerBot Mini Replicator. Table 3.2 defines the printing parameters for PETG.

The addition of glycol to polyethylene terephthalate helps the material to impart a smoother surface finish to the printed part. The only drawback of using PETG filament was extensive stringing.

The sieve like structure of the substrate was developed to increase available surface area for adsorption. The total area exposed is 206 cm^2 (Figure 3.4)

Table 3.2.
Printing parameters for PETG

Parameters	**Assigned Value**
Extrusion Temperature	230° C
Layer Height	0.01 mm
Printing Speed	10 mm/sec

Table 3.3.
Model details of substrate

Diameter	10 mm
Depth	5 mm
Channel size	2 mm

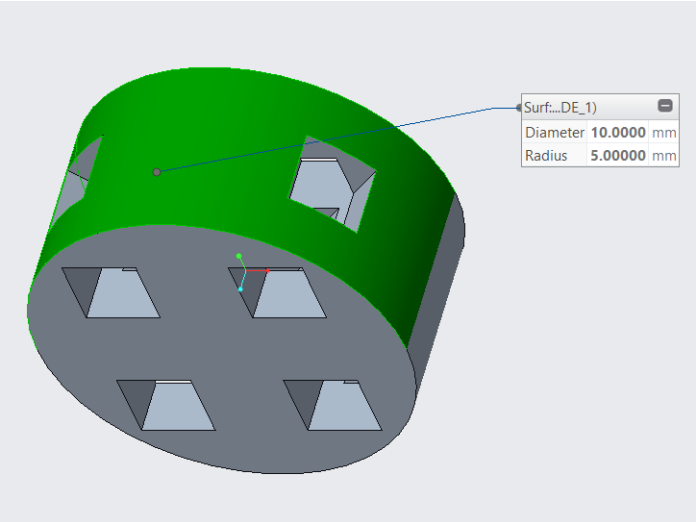

Fig. 3.2. CAD Model

3.3 Deposition of MIL-101 (Cr) Coating on PETG Substrate

MIL-101(Cr) coatings were developed on PETG substrates to impart MOF like properties to the substrate. It was executed based on a previous research [35]. Like

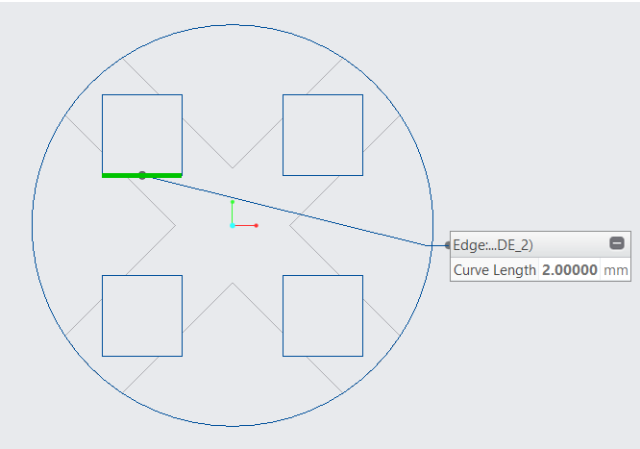

Fig. 3.3. Channel Size

Fig. 3.4. Additional Area

mentioned earlier in section 2.3, MOFs are not structurally stable and hence their applications is limited. But developing MOF coatings (in our case MIL-101 (Cr)) on a mechanically and structurally stable substrate will open a wide range of applications for MOFs and hence enable us to capture their full potential. A Layer by Layer (LbL) approach was incorporated to develop MIL-101 (Cr) coatings on PETG substrates. The LbL approach worked on the basic principle of electrostatic interactions. The substrates were dipped in an orderly fashion in two oppositely charged

Fig. 3.5. Printed PETG Disk Front View

Fig. 3.6. Printed PETG Disk Side View

solutions. MIL-101 (Cr), when dissolved in water forms a water stable dispersion of positively charged particles [35].The complementary species used for LbL assembly was poly(styrenesulfonate) (PSS) which forms a negatively charged solution when dissolved in water. LbL was carried out on the basis of a previous research [35]. The following are the steps undertaken for LbL assembly:

Fig. 3.7. PETG Filament-1.75 mm

Fig. 3.8. Makerbot Replicator Mini

- The pure MIL-101 (Cr) obtained was grounded and dispersed as nanoparticles in DI water and sonicated for 15 mins to obtain a homogeneous 0.75 wt% colloidal dispersion. This was further used as the stock solution.
- The stock solution was further diluted to make a working solution of 0.3 wt%.

- A 20×10^{-3} M aqueous solution was made using the complementary species PSS and DI water.
- Printed PETG substrates were repeatedly cleaned with acetone and DI water before proceeding with the LbL assembly.
- A layer of Branched Polyethyleneimine (B-PEI) was applied on the PETG substrates to promote good adhesion of the successive PSS and MOF layers.
- 1 wt% B-PEI solution was prepared with DI water for the adhesion promoting layer.
- The substrates were dipped in the B-PEI solution for 15 mins and then rinsed in three different steps of 2, 2 and 1 minutes respectively.
- The substrates were then air dried and stored in a clean place.
- The LbL assembly started by dipping the substrates in 20×10^{-3} M PSS solution for 15 minutes followed by rinsing as described in the previous step.
- The substrates were then dipped in the 0.3 wt% MIL-101 (Cr) working solution for 15 minutes followed by the rinsing steps defined earlier. The substrates were then air dried and stored in a clean place.
- The deposition of a layer of PSS and MIL-101 (Cr) constituted one layer pair. Desired number of layer pairs were then deposited on the substrates.

Please note that MIL-101 (Cr) and B-PEI form a positively charged solution whereas PSS forms a negatively charged solution. Also, B-PEI layer was just used in the beginning as an adhesion promoting layer. Following layer pairs comprised of MIL-101 (Cr) and PSS depositions only.

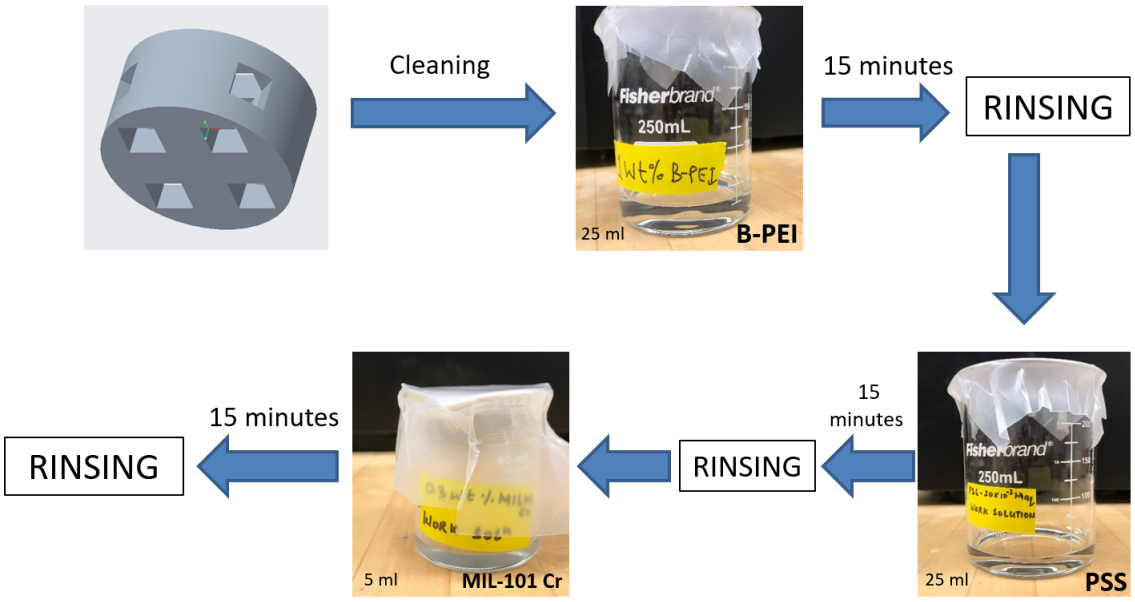

Rinsing: 2,1 and 1 minutes respectively with Di water and then drying with air.

Fig. 3.9. LbL Assembly

4. COMPUTATIONAL MODELING

With the advent of computer technology and molecular dynamics, and the development in computational sciences, it has become very convenient to simulate a physical model for its outcomes and predict its feasibility. This chapter is focused on developing models for nitrogen and carbon dioxide adsorption on MIL-101 (Cr). Rest of the details of the model would be discussed in depth in the upcoming sections.

4.1 Adsorption of Nitrogen and Carbon Dioxide on MIL-101 (Cr)

MIL-101(Cr) was used for this computational study because of its popularity in filtration applications. MIL-101 (Cr) has tetragonal chromium atoms acting as attraction sites and the organic ligands as connectors between these chromium atoms. MIL-101(Cr) was imported from Crystallography open database.It has a 3D triclinic type lattice and the lattice parameters are as stated in table 4.1. The structure is made up of chromium, hydrogen and oxygen atoms.

Table 4.1.
MIL-101(Cr) lattice parameters

Parameters	**Assigned Value**
A (Å)	88.86
B (Å)	88.86
C (Å)	88.86
α (degrees)	90
β (degrees)	90
γ (degrees)	90

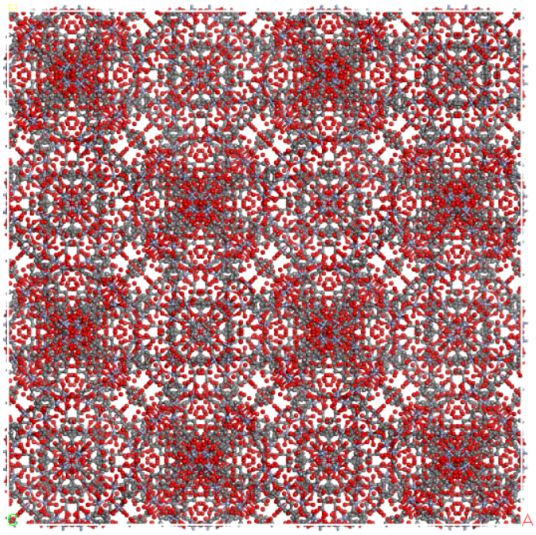

Fig. 4.1. MIL-101 (Cr) Lattice [36]

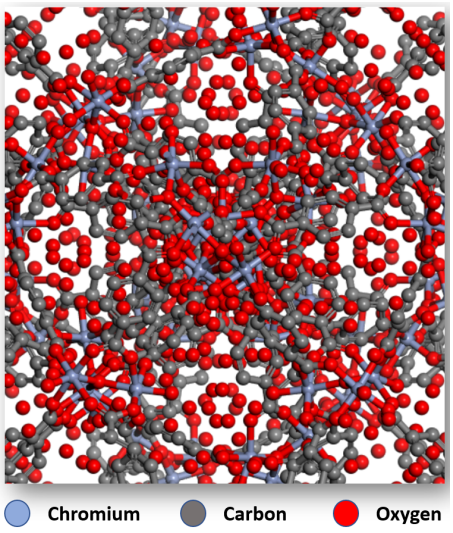

Fig. 4.2. MIL-101 (Cr) Lattice- Closeup

COMPASS force field was used to determine the interatomic interactions between the structure (adsorbent) and the gas (adsorbate). COMPASS incorporates expressions for bond lengths, bond angles, dihedrals, out-of-plane angles, coulombic forces and LJ potential. This force field is mostly used for modeling condensed phases and thermo-physical properties [37]. The model consists of 16120 atoms. Because of the

large number of atoms and their corresponding bonds, the model is computationally expensive. Inorder to make it feasible to run, the equilibration steps were reduced to 1000 from 100,000. The model calculates the adsorption isotherm using fugacity of the gas which considers real gases rather than ideal gases. The experimental BET isotherm is generally plotted for relative pressure ($\frac{P}{P0}$). Therefore, to match the cartesian system of the experimental plot, the relative pressure required was converted to fugacity. The relation between pressure and fugacity is given as follows:

$$f \propto P \tag{4.1}$$

$$f = \varphi P \tag{4.2}$$

where,

f = fugacity

P = applied gas pressure

φ = Fugacity coefficient

The vapor pressure for nitrogen is, $P_0 = 0.97$ bar. This was calculated using the Antoine equation [38] given as:

$$\log_{10}(P_0) = A - \frac{B}{C + T} \tag{4.3}$$

where,

A,B and C are predefined Antoine constants. They are listed in table 4.2 for Nitrogen and table 4.3 for Carbon dioxide.

Table 4.2.
Antoine constants for N_2

Temp. Range (K)	**A**	**B**	**C**
63.14 to 78	3.637	257.877	-6.344

Similarly, vapor pressure for carbon dioxide is, P_0= 1.11 bar. The relative pressure

Table 4.3.
Antoine constants for CO_2

Temp. Range (K)	**A**	**B**	**C**
63.14 to 78	3.637	257.877	-6.344

($\frac{P}{P_0}$) was then translated to fugacity using the above stated equations. The model was run for a fugacity value from 0.01 KPa to 103.5 KPa with 10 fugacity steps. The grid was kept at a default value of 0.4 Å.

Nitrogen

Nitrogen molecule was constructed as a 3D atomistic model. It was then optimized using the Forcite model to minimize the interatomic forces and get all the atoms in a state of equilibrium. The energy was minimized to 0.0001 Kcal/mol and force was minimized to 0.005 Kcal/mol/Å. COMPASS was used as the forcefield.
The bond length was kept as 1.48 Å. The initial energy of the molecule was 141.82 Kcal/mol. The optimized molecule geometry was used as the adsorbate species for running the adsorption model.

Carbon dioxide

A similar approach was incorporated in developing carbon dioxide molecule. The bond length was 1.51 Åbetween the carbon atom and oxygen atom. All the other parameters were kept the same as for nitrogen molecule for optimising the molecule geometry. The energy before optimization was 216.39 Kcal/mol. The optimised CO_2 molecule was then used for studying the adsorption on MIL-101 (Cr) surface.

5. RESULTS AND DISCUSSION

In this section, the in-house synthesised MIL-101 Cr and the coated substrates were analysed for their micro-structure, composition and adsorption capacity. All of the stated would be discussed further in depth in their particular subsections. Computational models developed for N_2 and CO_2 adsorption would also be discussed in this section.

5.1 MIL-101 (Cr) Powder Characterizations

SEM analysis was carried out to study the micro-structure of the synthesized MIL-101 powder followed by an XRD analysis to study if any phase change was detected. Three different samples A, B and C were analysed. All the three samples were synthesized using the same procedure listed in section 3.1 Table 5.1specifies the sample weights.

Table 5.1.
Sample weights of MIL 101 (Cr) powder

Sample	**Weight**
Sample A	28.4 mg
Sample B	193.1 mg
Sample C	12 mg

5.1.1 SEM Results

As can be seen from the SEM figures at different magnifications (Figures 5.1 to 5.9), MIL-101 (Cr) has acicular shape. If observed closely in Figure 5.1 the particles

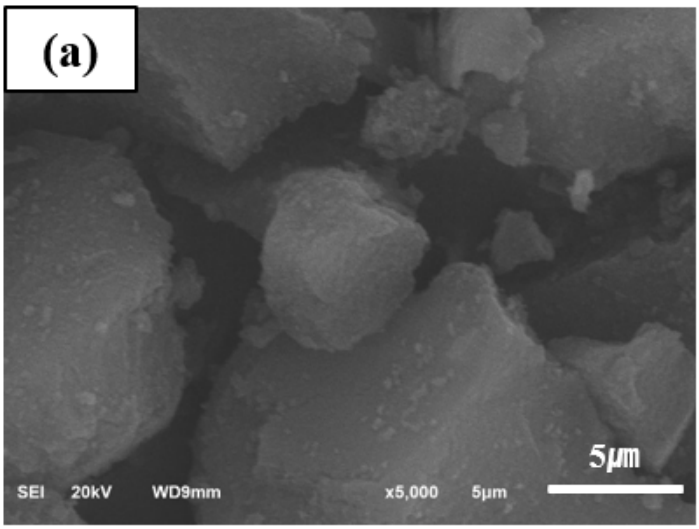

Fig. 5.1. MIL 101 (Cr) SEM 5μm - *Sample A*

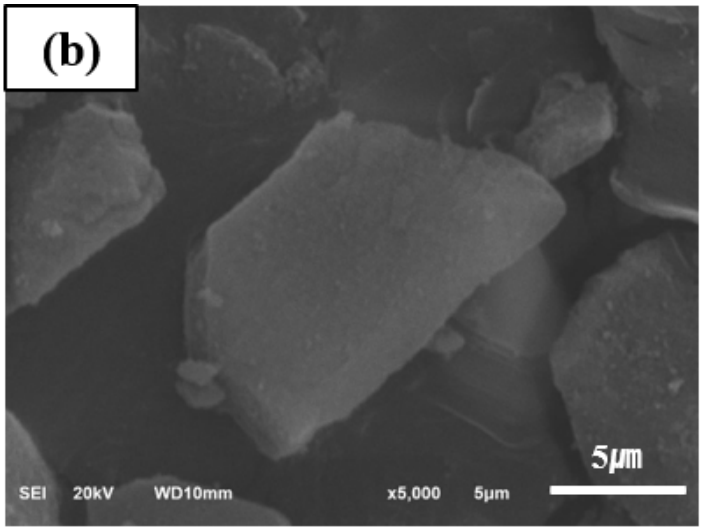

Fig. 5.2. MIL 101 (Cr) SEM 5μm - *Sample B*

appear to be of octahedron geometry. This can be attributed to the presence of chromium atoms at the nodes. The SEM for MIL-101(Cr) can be verified from a previously reported research [39] in Figure 5.10

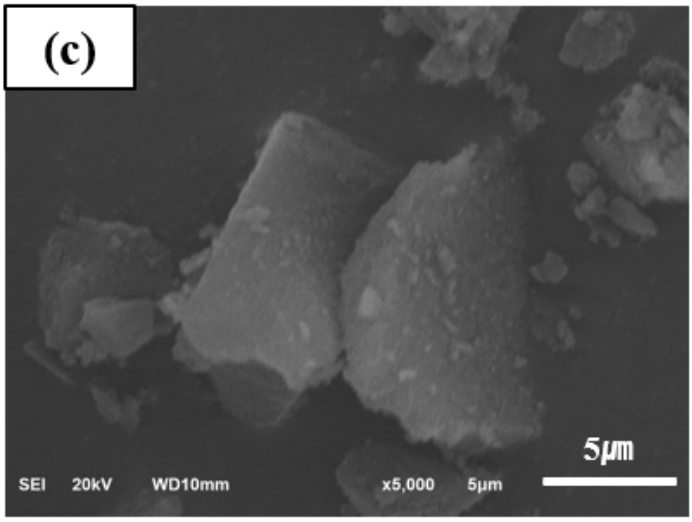

Fig. 5.3. MIL 101 (Cr) SEM 5μm - *Sample C*

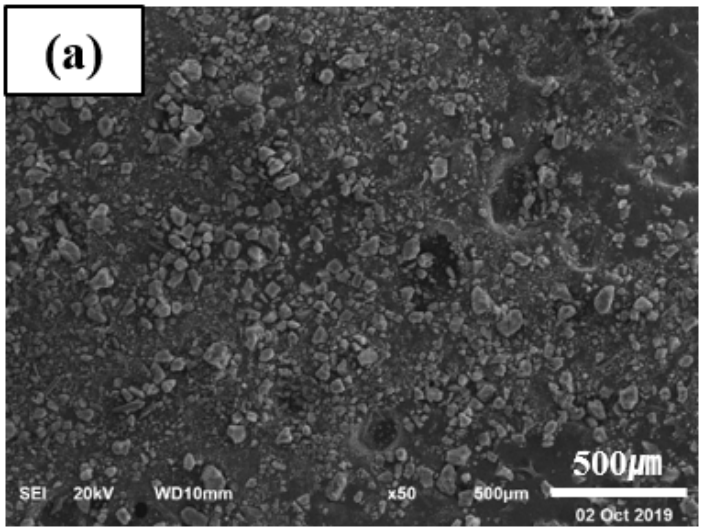

Fig. 5.4. MIL 101 (Cr) SEM 500μm - *Sample A*

5.1.2 XRD Results

All the three samples were tested for composition and phase change using XRD analysis. It can be observed that all the samples have a uniform composition and that all of them maintain their crystalline form and hence are stable. The XRD results

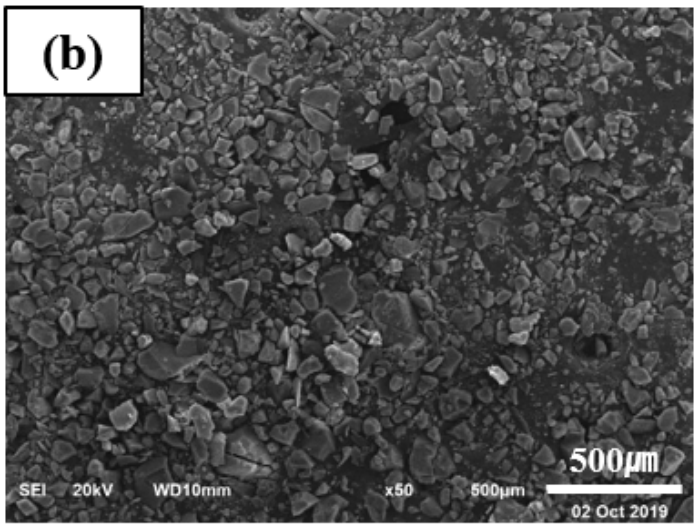

Fig. 5.5. MIL 101 (Cr) SEM 500μm - *Sample B*

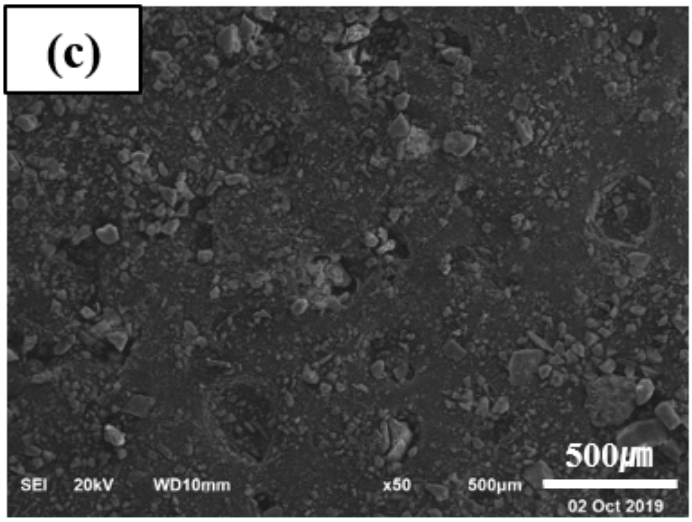

Fig. 5.6. MIL 101 (Cr) SEM 500μm - *Sample C*

can be verified from the same reference that was used for preparing MIL-101 (Cr) coatings (Figure 5.12).

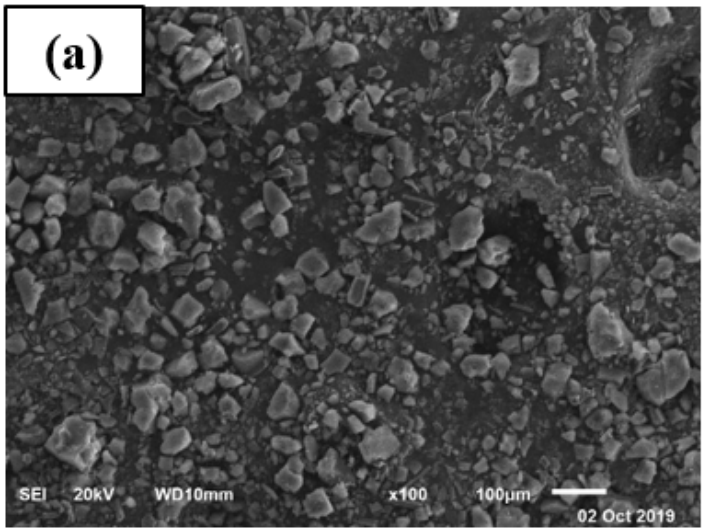

Fig. 5.7. MIL 101 (Cr) SEM 100μm - *Sample A*

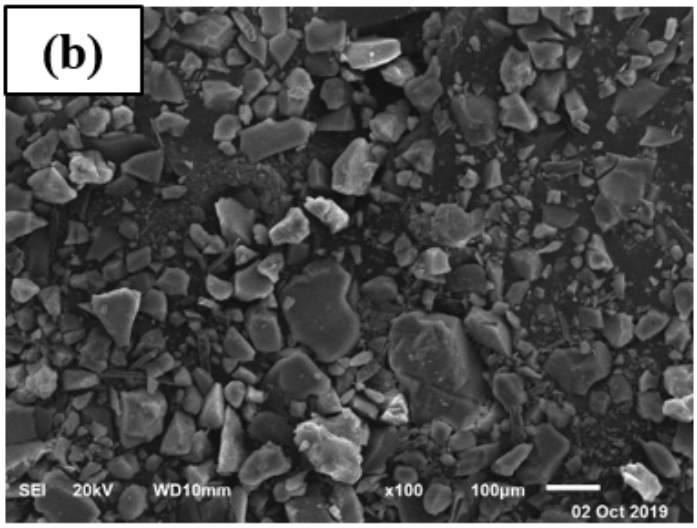

Fig. 5.8. MIL 101 (Cr) SEM 100μm - *Sample B*

5.2 MIL 101 (Cr) Coated on PETG Substrates

The printed PETG substrates were coated with MIL 101 (Cr) by following the LbL procedure specified in section 3.3. The substrates were coated with 10, 20 and 30 layer pairs respectively. One substrate was left as printed and that acted as the control. Apart from the substrates, a segment of PETG filament was also coated with

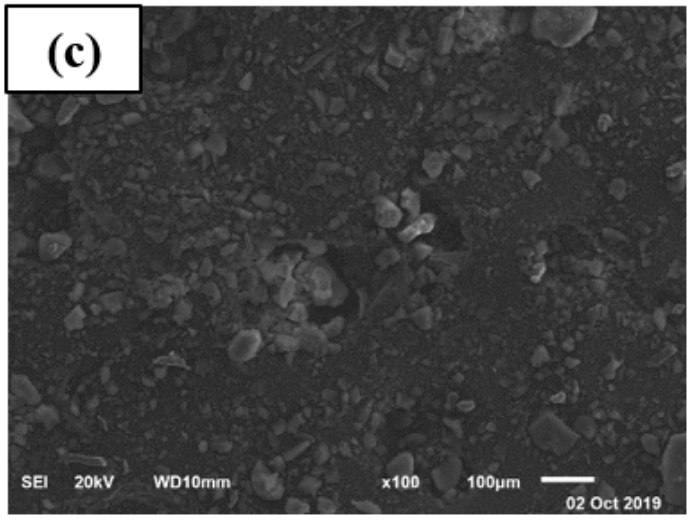

Fig. 5.9. MIL 101 (Cr) SEM 100μm - *Sample C*

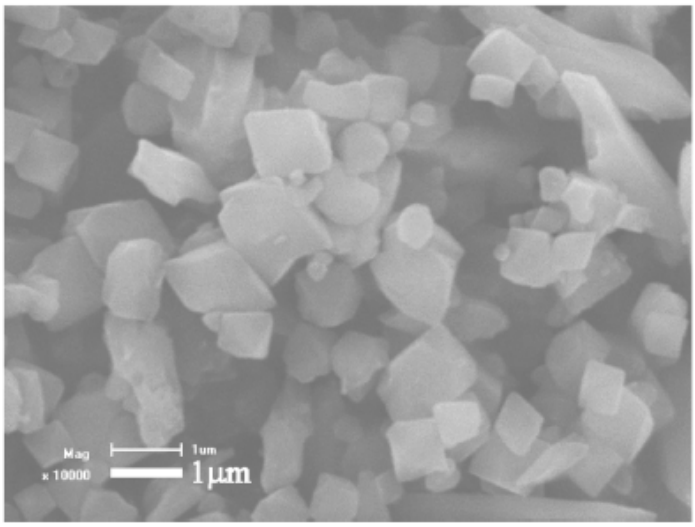

Fig. 5.10. MIL 101 (Cr) SEM 1μm - Reference

15 layer pairs. This was done to observe the deposition of MIL-101 (Cr) at the cross section

The following subsections show the SEM analysis of control and coated substrates and the coated PETG filament cross section.

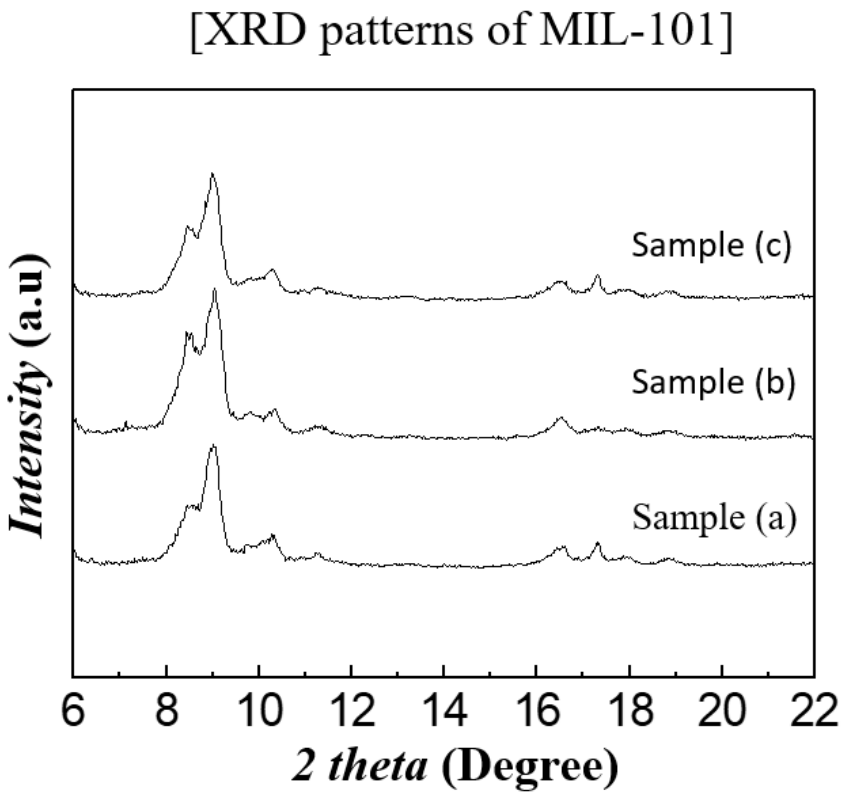

Fig. 5.11. XRD Analysis of Different MIL 101 (Cr) Samples

5.2.1 SEM and EDS Analyses

It can be noted from the EDS analysis that no chromium is present on the substrate. Also on observing the SEM images at different magnifications, no coating is visible. Carbon accounts for almost 85% of the atomic composition and Oxygen accounts for almost 15% of the atomic composition. This fact should be duly noted as it helps in analysing the composition and determining if there is any change in the composition due to addition of MIL-101 (Cr) layers.

A slight dilation of the PETG fibers can be observed but its not uniform.This can be because of uptake of moisture at certain locations caused by the water based assembly of LbL layers. No visible coating layers can be observed. However the EDS data shows the presence of chromium which validates the deposition of MIL-

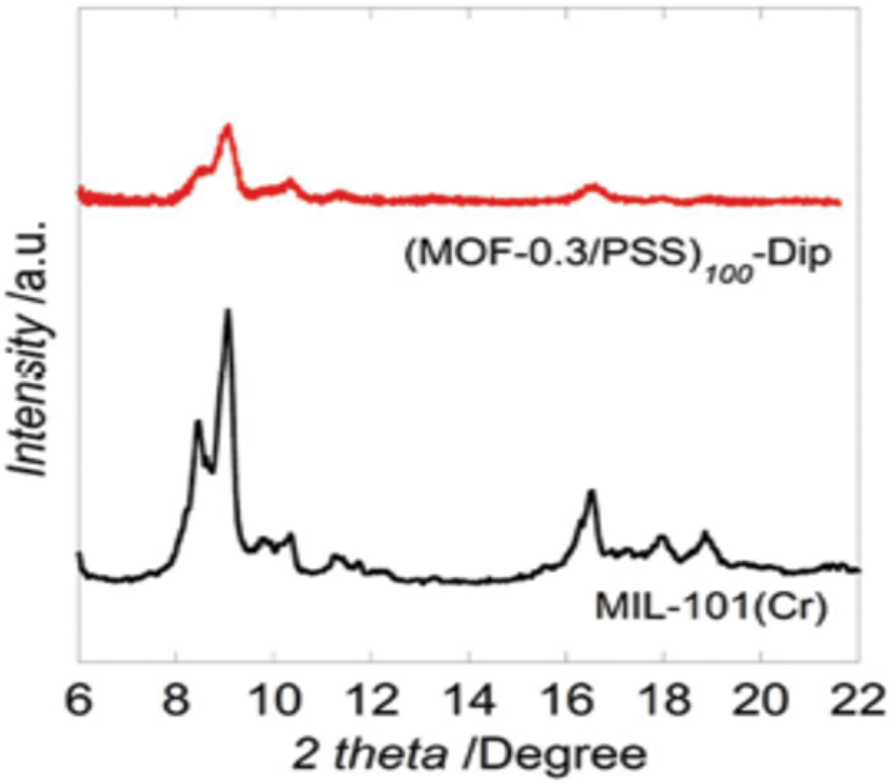

Fig. 5.12. XRD Analysis of MIL-101 (Cr)- Reference [35]

101(Cr) on the substrate. It can also be noted that the atomic percentage of Carbon and oxygen remains the same which indicates towards the fact that the addition of MIL-101 (Cr) coatings do not affect the composition of the substrate.

At 20 layers, the dilation of the PETG fibers is aggravated. However it is still not uniform. Some locations show a glimpse of coated layers, but it is not distinctly visible. The EDS data shows presence of chromium which validates the successful deposition of MIL-101 (Cr). There is no change in the composition of the substrate.

The dilation of PETG fibre looks uniform. At 30 layers, the coating is distinctly visible on the substrate. The EDS data shows a rise in chromium percentage. This increase in chromium content bolsters the fact that increasing the number of layer pairs account for increased deposition of MIL-101 (Cr) on the substrate.

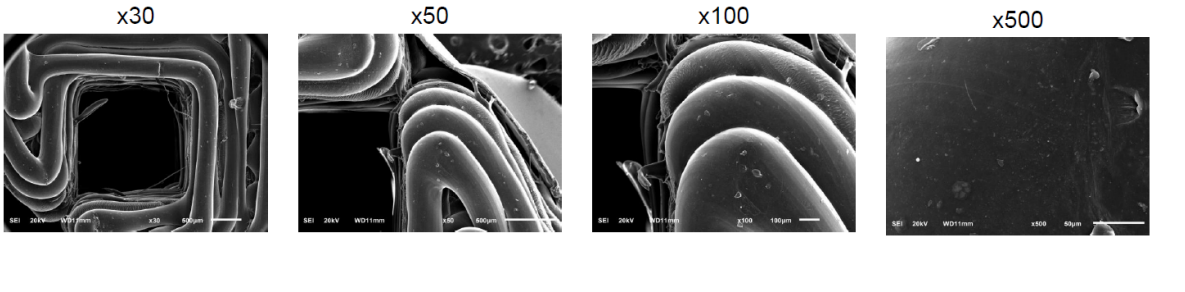

Element	Wt%	Wt% Sigma	Atomic %
C	80.64	0.33	85.18
O	17.84	0.32	14.15
Na	0.50	0.03	0.28
Si	0.36	0.02	0.16
Cl	0.53	0.02	0.19
K	0.14	0.02	0.04

Element	Wt%	Wt% Sigma	Atomic %
C	82.20	0.51	86.02
O	17.80	0.51	13.98
S	0.00	0.04	0.00
K	0.00	0.03	0.00

Fig. 5.13. PETG Disk as Printed

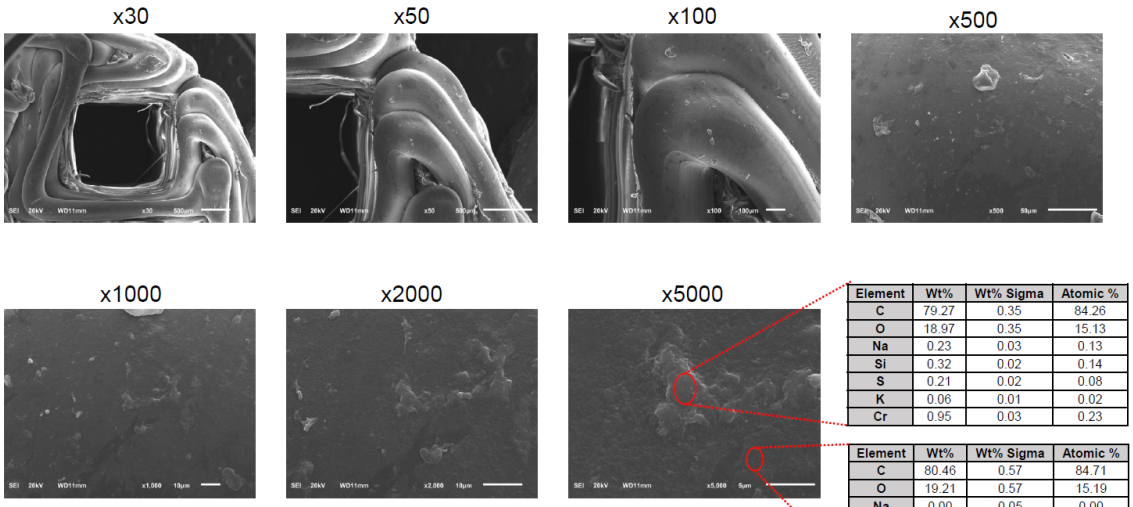

Element	Wt%	Wt% Sigma	Atomic %
C	79.27	0.35	84.26
O	18.97	0.35	15.13
Na	0.23	0.03	0.13
Si	0.32	0.02	0.14
S	0.21	0.02	0.08
K	0.06	0.01	0.02
Cr	0.95	0.03	0.23

Element	Wt%	Wt% Sigma	Atomic %
C	80.46	0.57	84.71
O	19.21	0.57	15.19
Na	0.00	0.05	0.00
Si	0.09	0.03	0.04
K	0.00	0.02	0.00
Cr	0.24	0.04	0.06

Fig. 5.14. MIL 101 Coated Disk-10 Layers

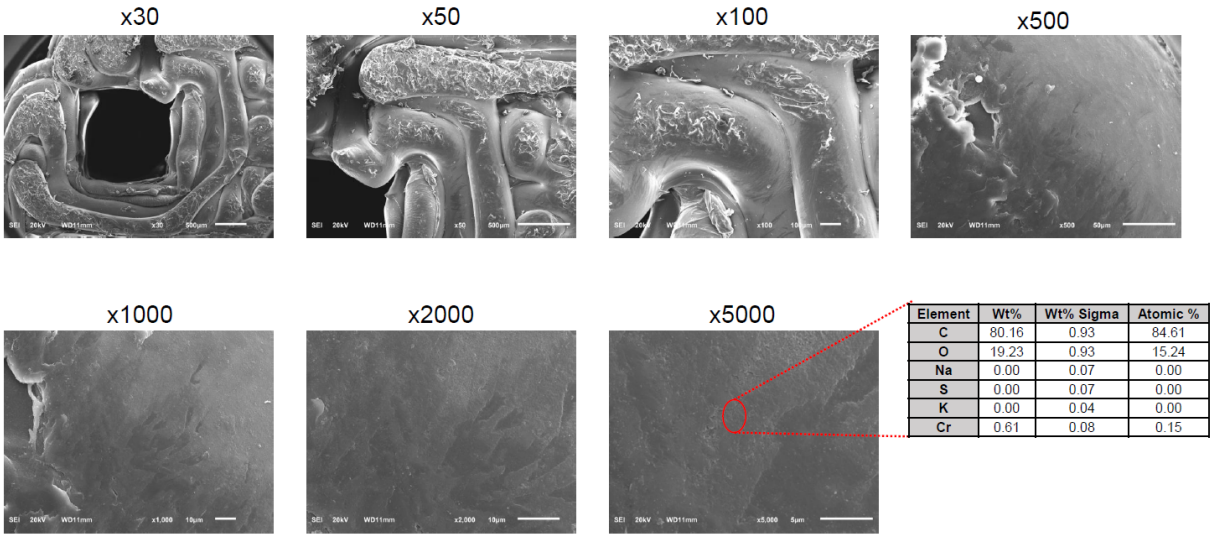

Element	Wt%	Wt% Sigma	Atomic %
C	80.16	0.93	84.61
O	19.23	0.93	15.24
Na	0.00	0.07	0.00
S	0.00	0.07	0.00
K	0.00	0.04	0.00
Cr	0.61	0.08	0.15

Fig. 5.15. MIL 101 Coated Disk-20 Layers

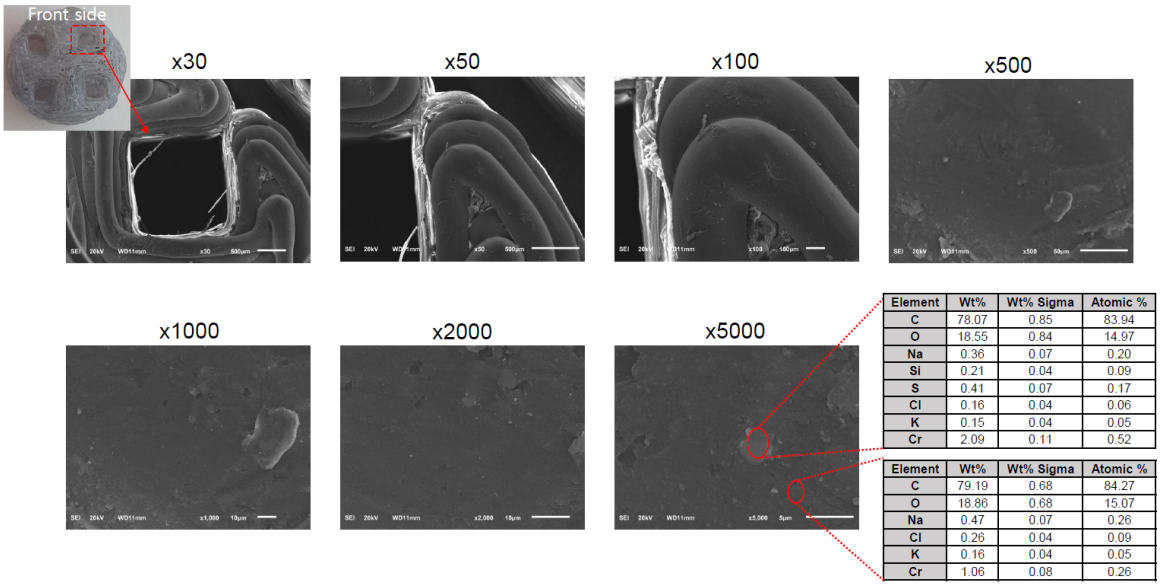

Element	Wt%	Wt% Sigma	Atomic %
C	78.07	0.85	83.94
O	18.55	0.84	14.97
Na	0.36	0.07	0.20
Si	0.21	0.04	0.09
S	0.41	0.07	0.17
Cl	0.16	0.04	0.06
K	0.15	0.04	0.05
Cr	2.09	0.11	0.52

Element	Wt%	Wt% Sigma	Atomic %
C	79.19	0.68	84.27
O	18.86	0.68	15.07
Na	0.47	0.07	0.26
Cl	0.26	0.04	0.09
K	0.16	0.04	0.05
Cr	1.06	0.08	0.26

Fig. 5.16. MIL 101 Coated Disk-30 Layers

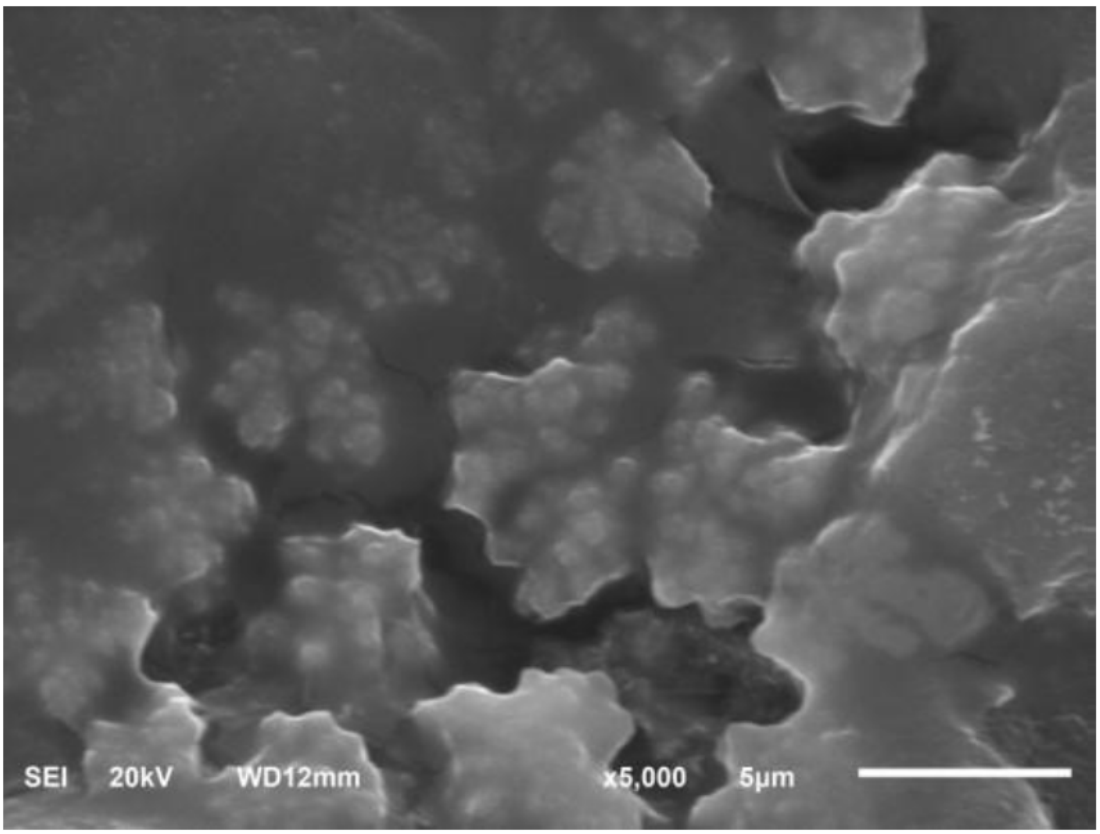

Fig. 5.17. MIL 101 Coated PETG Filament-15 Layers

MIL-101 (Cr) coatings are vividly displayed on the PETG filament. Clusters of octahedral MIL-101 (Cr) can be seen deposited on PETG surface. These clusters become active sites for adsorption.

It can be concluded from the EDS results that deposition of MIL-101 (Cr) coatings was successful. However the presence of chromium III which acts as the binding site for gas molecules is not uniform on the coated surface.

5.3 BET Analysis

BET analysis was carried out on MIL-101 (Cr) powder to understand its adsorption characteristics and also to get the BET specific area. BET specific area determines the number of available sites for possible adsorption. The higher the BET

specific area is, the higher is the adsorption potential of the material. The same three samples from section 5.1 were used to run the test. All the samples were pretreated by heating at 150° C for 4 hours. The pretreatment was followed by degassing to remove any adsorbed impurities. Nitrogen was used as the adsorptive specie at 77K. The results for *Sample C* could not be determined due to the small quantity of available powder.

The following sections discuss the BET analysis results and compare the experimental data with the computational data.

5.3.1 MIL-101 (Cr) Experimental Results

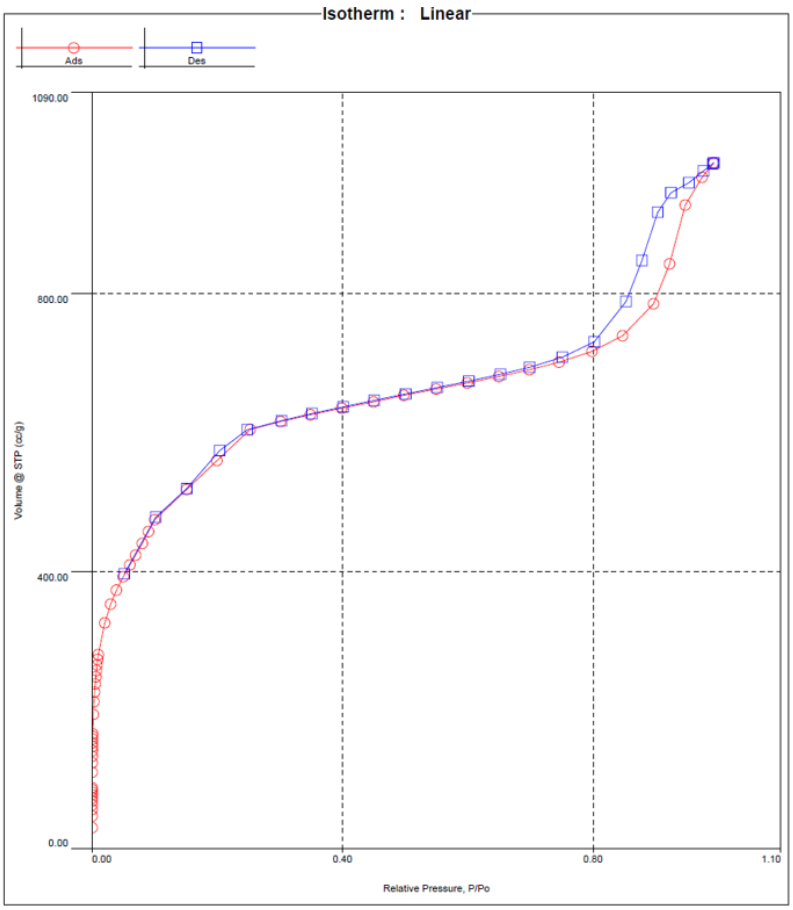

Fig. 5.18. Adsorption Isotherm- Sample A

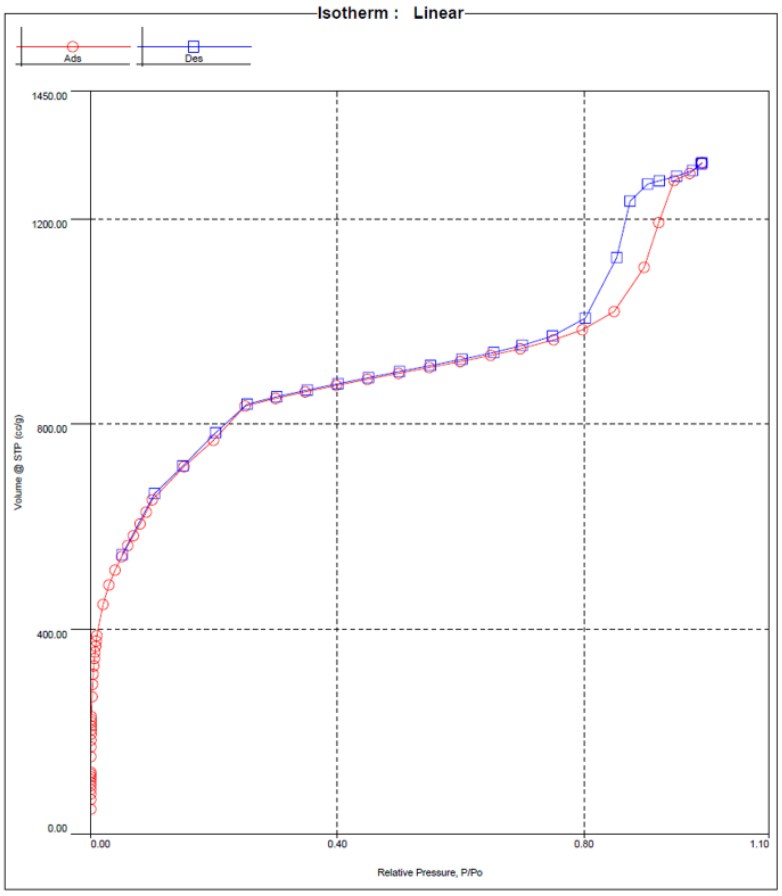

Fig. 5.19. Adsorption Isotherm- Sample B

Both the isotherms- sample A and sample B follow a similar trend which account towards the uniformity of the powder. A high uptake at low relative pressures ($\frac{P}{P_0}$= 0 to 0.3) indicates adsorption in mesopores of MIL-101 (Cr). As the relative pressure increases, the uptake of nitrogen flat lines before escalating rapidly again at high relative pressures. This can be justified by the fact that the first layer of nitrogen is adsorbed before entering the medium relative pressure levels. Beyond this, the subsequent accumulation of nitrogen molecules start on the already adsorbed first layer and the system then enters into multilayer adsorption. The first layer is the true absorbed layer as it is established at the solid-gas interface. The subsequent layers are adsorbed at the previously adsorbed gas layer thereby normalising the adsorption curve. Further when the partial pressure value increases, there is a sudden increase

in the adsorbed gas volume. This is because as the partial pressure P_0 approaches the saturation pressure P the system then enters into bulk condensation phase.
The data from the experiments was fitted using a built in MATLAB function for linear curve fitting and the resulting curve was used in determining the heat of desorption ($\Delta_{des}H$). Linear curve fitting was used inorder to calculate the slope and intercept of the line which would then be used for further findings. ($\Delta_{des}H$) helps to determine the feasibility of adsorption. For a molecule to be successfully adsorbed onto a substrate, its heat of vaporisation ($\Delta_{vap}H$) should be less than ($\Delta_{des}H$). Figure 5.21 shows the BET linear plot for sample A. The MATLAB code for linear curve fit is as follows:

```
% Experimental Data
x= [4.69E-02 5.76E-02 6.61E-02 7.89E-02 8.74E-02 9.81E-02 1.49E-01 1.96E-01 2.49E-01 2.98E-01 3.48E-01];
y= [3.96E+02 4.11E+02 4.26E+02 4.44E+02 4.62E+02 4.77E+02 5.23E+02 5.65E+02 6.09E+02 6.20E+02 6.31E+02 ]; const= lsqcurvefit(@f,[0;0],x,y); % MATLAB function for linear curve fit
% @f is user defined function- y= mx + c
m=const(1);
c=const(2);

xfit=0.0469:0.05:0.35;
yfit=f(const,xfit);

figure
plot(x,y,'-.b*')
hold on
plot(xfit,yfit,'r','linewidth',2)
grid on
```

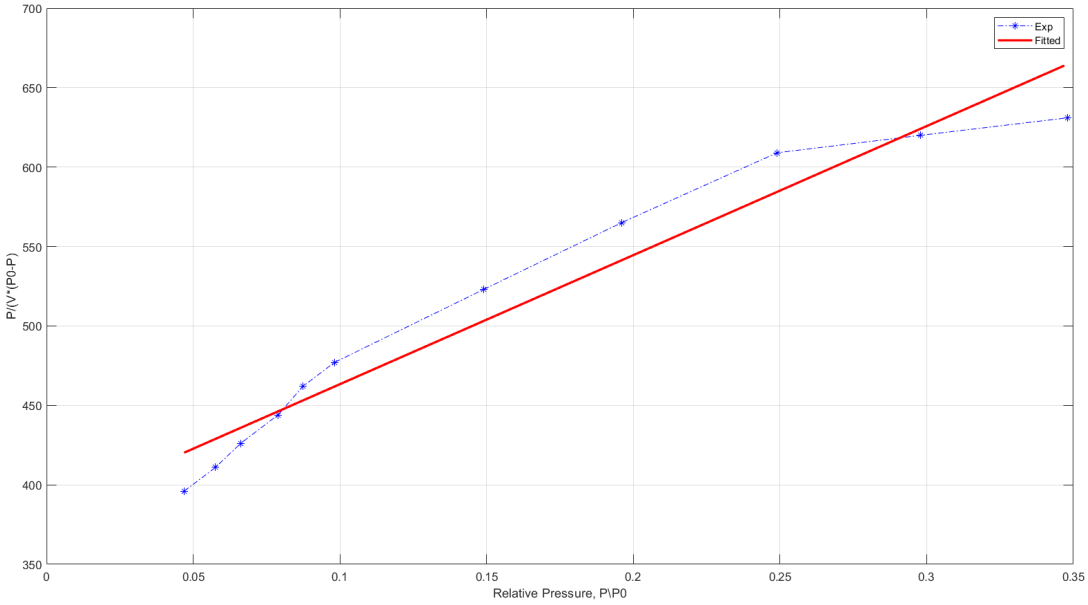

Fig. 5.20. BET Linear Plot- Sample A

The range for relative pressure, $\frac{P}{P_0}$ was 0.05 to 0.35. This range is claimed to cover the monolayer coverage as per a previous research [18]. The slope of the fitted line as calculated is, m= 812.13 cc/gm and the y intercept, b= 382.15 cc/gm for sample A and m= 1090 cc/gm and b= 524.21 cc/gm for sample B.

Equation 2.3 was used to calculate the heat of desorption. The following relations were used to evaluate the value of C.

m= $(\frac{C-1}{V_m C})$

b= $\frac{1}{V_m C}$

$$C = exp^{\frac{\Delta_{des}H - \Delta_{vap}H}{R*T}} \tag{5.1}$$

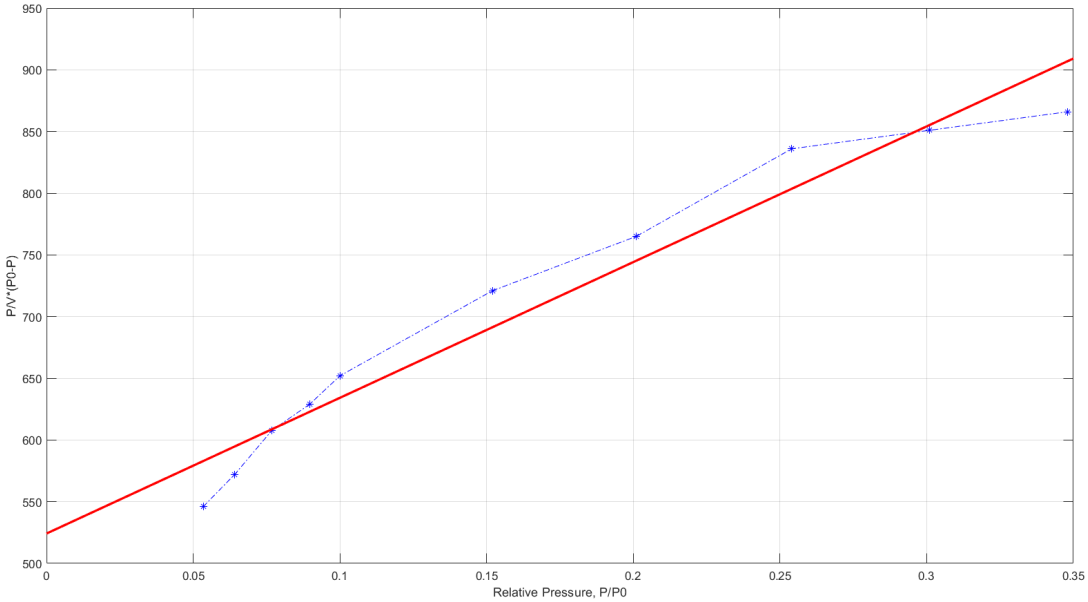

Fig. 5.21. BET Linear Plot- Sample B

or

$$\ln C = (\frac{\Delta_{des}H - \Delta_{vap}H}{R * T})$$

Therefore,

$\Delta_{des}H = \Delta_{vap}H + RTlnC$,

where,

$\Delta_{vap}H$ = 5.6 KJmol^{-1}

R = 8.314 J$mol^{-1}K^{-1}$

T = 77 K

After plugging in the respective values $\Delta_{des}H$ was calculated as 6.32 KJ mol^{-1} for sample A and $\Delta_{des}H$= 6.31 KJ mol^{-1} for sample B .

The value of $\Delta_{des}H$ is more than $\Delta_{vap}H$ in both the samples which proves that the adsorption of nitrogen on MIL-101 (Cr) is practical and feasible. The BET surface area calculated experimentally for both the samples show high coverage of nitrogen

on MIL-101 (Cr). The BET surface area for Sample A is 1616.43 $\frac{m^2}{gm}$ and for Sample B is 2716.83 $\frac{m^2}{gm}$. The difference in BET surface areas for both the samples is due to different sample weights. Both the samples show high BET surface areas thereby proposing MIL-101 (Cr) as a promising candidate for gas adsorption applications.

5.4 Modeling of Adsorption of Nitrogen and Carbon Dioxide on MIL-101 (Cr)

As discussed earlier in section 4.1, the simulation ran using nitrogen and carbon dioxide gases as adsorbates respectively. We will now evaluate the adsorption isotherm for gauging the uptake of both the gases. (Figure 5.22).

Adsorption of N_2 and CO_2 on MIL-101 (Cr) surface

The computational isotherm shows good uptake for nitrogen at low relative pressures starting with around 200 molecules of nitrogen per unit cell at P/P_0= 0.1. The computational result also follows the experimental trend thereby validating the experimental data. There is steep increase in the uptake observed at higher values of relative pressure, beyond P/P_0= 0.7 because as 'P' approaches 'P_0', the system enters in the bulk condensation phase and the gas molecules turn into liquid and start accumulating in the mesopores on MIL-101(Cr) surface. The computational result approves of the trend of the experimental data, however the middle range for relative pressure, i.e. $0.3 \leq \mathrm{P}/P_0 \leq 0.7$ does not completely agree to the experimental data that shows the multilayer adsorption phase. This is because of the less number of equilibration steps used to run the model.

Carbon dioxide, on the other hand shows a steady increase in uptake as the relative pressure increases, almost a linear trend. When compared with nitrogen, the difference in uptake is not much in the early values of relative pressure. As the relative pressure increases, the difference between the uptake of both the species start growing. The maximum difference is observed as P approaches P_0. This can be due to

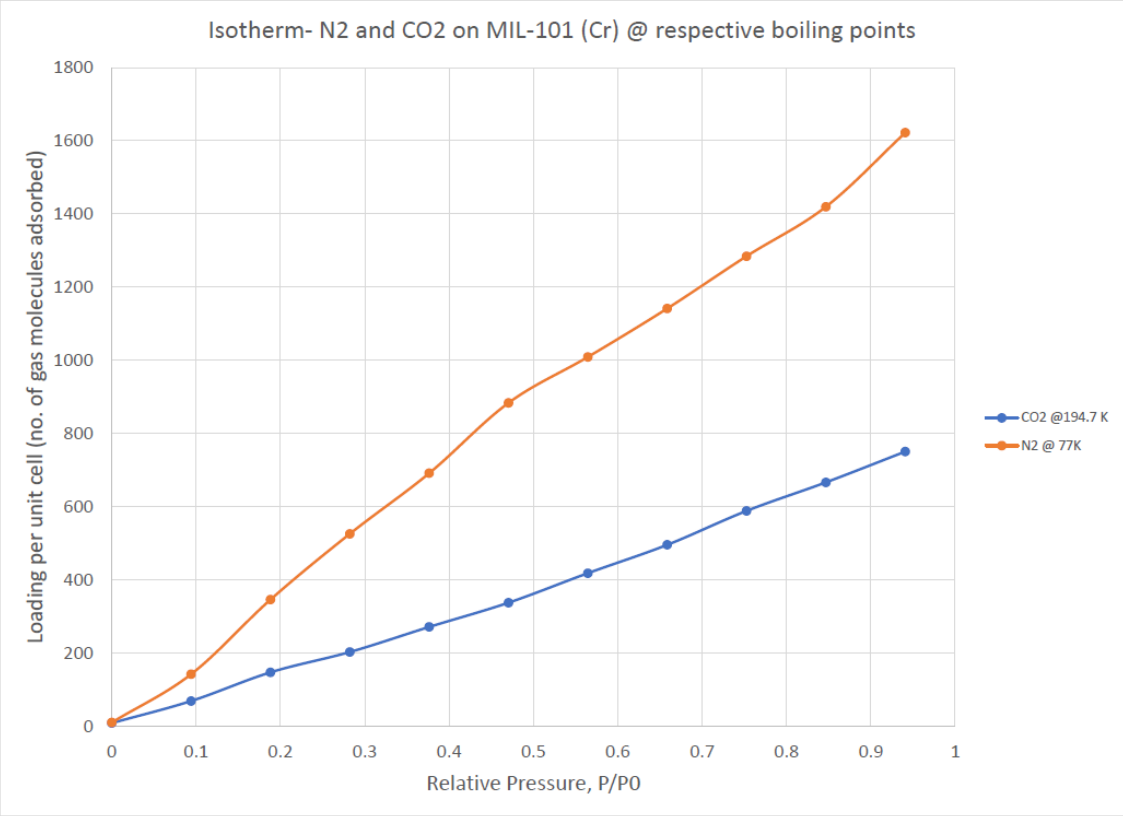

Fig. 5.22. Computational Isotherm for N_2 and CO_2 Adsorption on MIL-101 (Cr) at Respective Boiling Points

the difference in the molecular sizes of both the species. Carbon dioxide molecules being larger in size compared to nitrogen molecules occupy more area on MIL-101(Cr) as compared to the same number of nitrogen molecules. As a result, MIL-101 (Cr) surface saturates faster and with much less molecules adsorbed for carbon dioxide. The next set of figures would distinctively show the adsorption spots based on the energy of the adsorbate molecules.

As stated earlier, adsorption is an exothermic process. So when an adsorptive molecule adsorbs on the surface of the adsorbent, it forms a bond with the the surface molecules and release some energy. In figure 5.23, the blue spots represent negative energy spots. As the fugacity steps progress, the number of blue spots increase- showing the increase in uptake of nitrogen molecules.

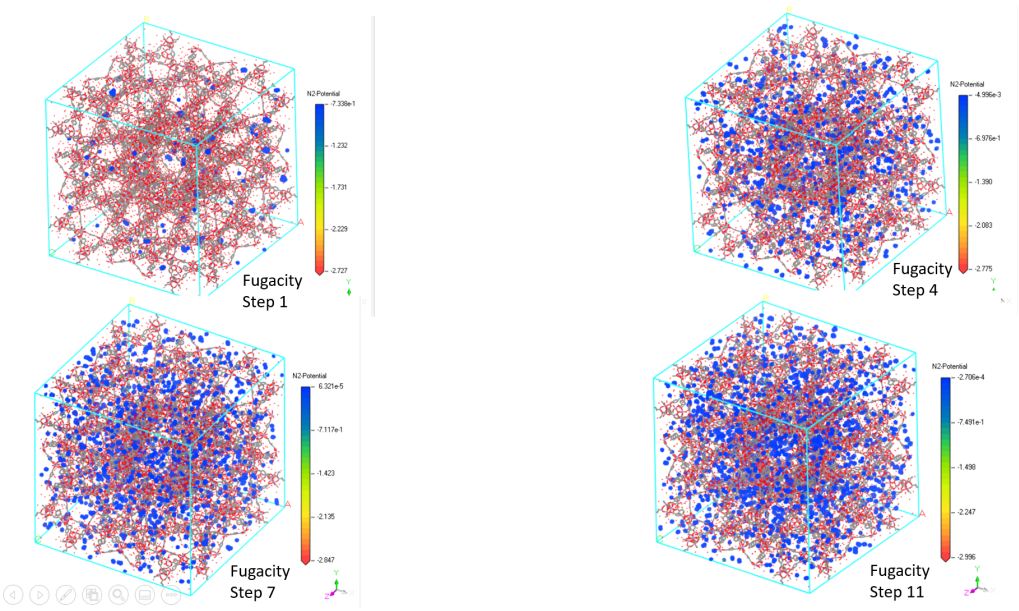

Fig. 5.23. Adsorption Locations for N_2 @ 77 K on MIL-101(Cr) Surface

Figure 5.24 depicts a closer view of the previously spotted adsorption locations. If observed carefully, fugacity step 1 shows a few green dots. These green dots are also negative energy spots but they are much lower in energy than the blue spots. This suggests towards the fact that, the green or the orange spots represent adsorption of nitrogen molecules on the surface of MIL-101 (Cr) whereas the blue spots represent adsorption on the previously adsorbed nitrogen molecules.

As the fugacity steps progress, we see fewer green and orange spots with almost none in fugacity step 11. This indicates towards multilayer adsorption. Similarly, figures 5.25 and 5.26 represent the same phenomenon for carbon dioxide.

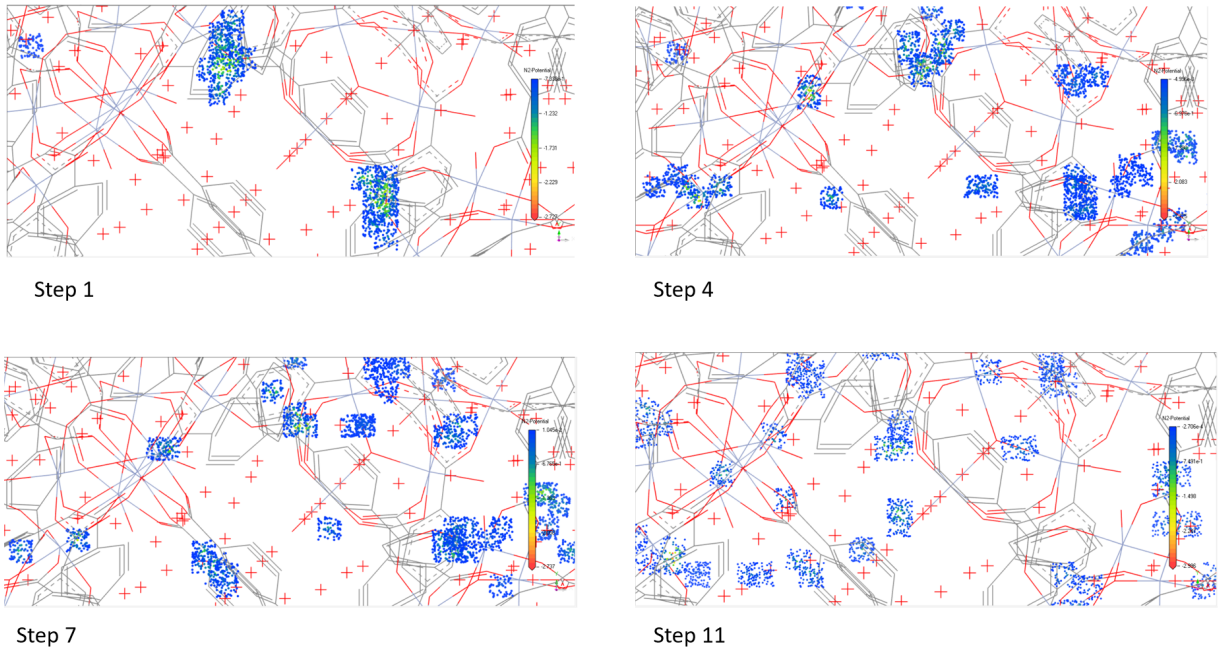

Fig. 5.24. Detailed View for Adsorption Locations for N_2 @ 77 K on MIL-101(Cr) Surface

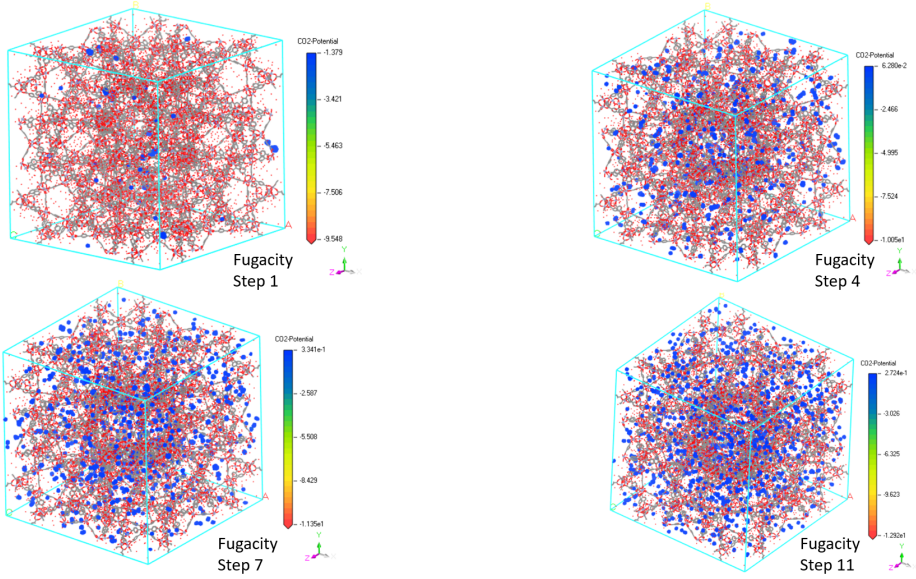

Fig. 5.25. Adsorption Locations for CO_2 @ 194.7 K on MIL-101(Cr) Surface

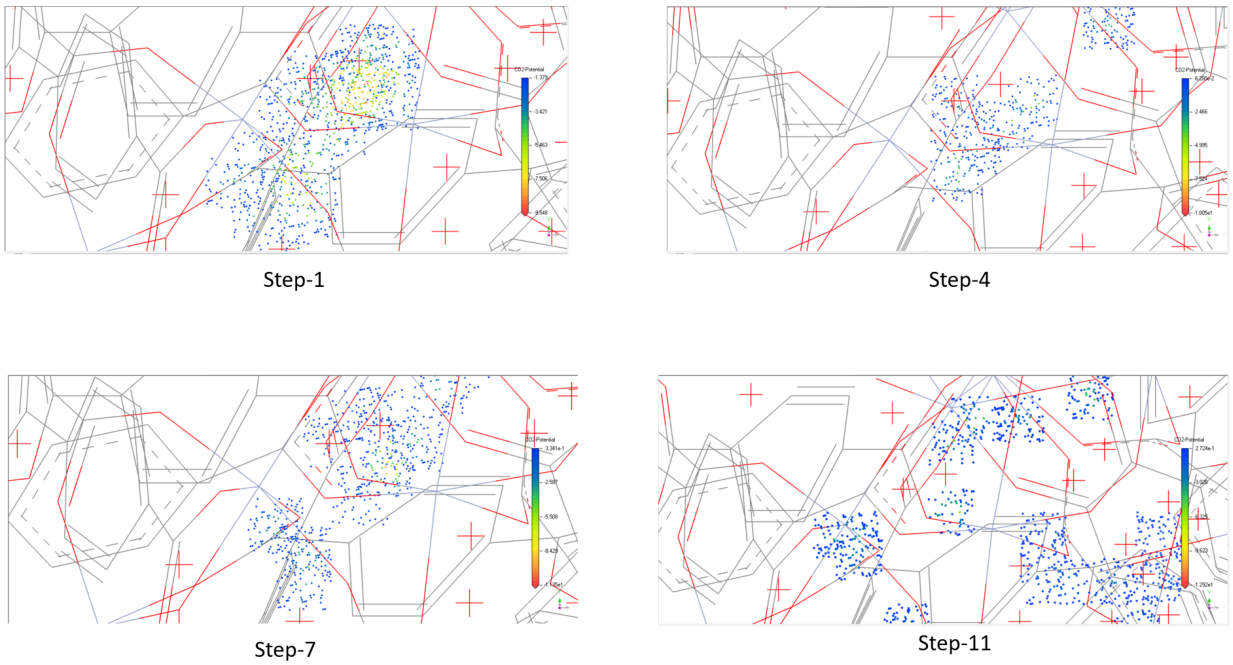

Fig. 5.26. Detailed View for Adsorption Locations for CO_2 @ 194.7 K on MIL-101(Cr) Surface

6. CONCLUSION

- MIL-101 (Cr), a chromium based MOF was selected for this study. MIL-101 (Cr) was successfully synthesized in house following a predefined procedure.

- MOFs exist in powder form. In order to apply them in actual applications, they were deposited on PETG substrate by using a layer by layer approach. A total of 30 layer pairs were deposited on PETG substrates. These coatings imparted MOF like properties to PETG printed substrates.

- Synthesized MIL-101 (Cr) was evaluated for nitrogen adsorption and displayed high uptake of nitrogen at low pressure (around 400 cc/gm @P/P0=0.05) with a peak of around 1000 cc/gm @P/P0 close to 1.

- BET single point surface area analysis expressed a high surface area (2716.83 m^2/gm) for MIL-101(Cr). Such a high BET area makes it a favorable surface for adsorption purposes.

- SEM results showed that MIL-101 (Cr) particles are octahedral and XRD data exhibited crystalline structure all throughout the samples with no phase change.

- Coated samples showed presence of chromium in EDS analysis which bolstered the adhesion of layer pairs on PETG substrates. However, the coated surfaces showed an uneven presence of chromium III which act as the binding sites for gas molecules. Further investigation and improvement in the coating process is needed to aid in a much even and smoother deposition of chromium III on the coated surface.

- A computational model was developed to study and evaluate the adsorption of nitrogen and carbon dioxide on MIL-101 (Cr) surface.Nitrogen adsorption

validated the experimental results whereas the latter served as a fundamental scope for carbon dioxide adsorption performance. The uptake of carbon dioxide was less as compared to nitrogen due the difference in molecular sizes of both the species.

- The computational models presented a reasonable estimate of adsorption sites based on low energy areas.

7. CONTRIBUTIONS OF WORK

- MIL-101 (Cr) MOF was deposited as coatings on 3D printed PETG substrates to impart MOF like properties to the substrate. This helped in addressing the processability issue with MOFs.
- Computational models were developed to evaluate adsorption of nitrogen and carbon dioxide on MIL-101 (Cr) surface. The models displayed good uptake of both the gases thereby proposing MIL-101 (Cr) as a promising candidate for gas adsorption applications.

8. FUTURE WORK

- Evaluate MIL-101 (Cr) for carbon dioxide adsorption.
- Improve the accuracy of computational models by using a reasonable amount of equilibration steps.
- Develop a composite material and by mixing metal organic frameworks and zeolite and test it for adsorption capabilities.

REFERENCES

REFERENCES

[1] L. Alaerts, F. Thibault-Starzyk, E. Séguin, J. F. Denayer, P. A. Jacobs, and D. E. De Vos, "Mof materials as catalysts for organic transformations and as selective hosts in recognition of organics," in *Studies in surface science and catalysis*. Elsevier, 2007, vol. 170, pp. 1996–2003.

[2] A. C. Caputo, P. M. Pelagagge, and P. Salini, "Impact of accidents risk on hydrogen road transportation cost," *International Journal of Energy Sector Management*, 2011.

[3] G. D. Berry, "Hydrogen as a transportation fuel: costs and benefits," Lawrence Livermore National Lab., CA (United States), Tech. Rep., 1996.

[4] T. Halvorson, C. Terbot, and M. Wisz, "Hydrogen production and fueling system infrastructure for pem fuel cell-powered vehicles," *Praxair, Inc. for the Ford Motor Company*, vol. 12, 1996.

[5] M. Qadrdan, Y. Saboohi, and J. Shayegan, "A model for investigation of optimal hydrogen pathway, and evaluation of environmental impacts of hydrogen supply system," *International journal of hydrogen energy*, vol. 33, no. 24, pp. 7314–7325, 2008.

[6] P. K. Sahoo, M. John, B. L. Newalkar, N. Choudhary, and K. Ayappa, "Filling characteristics for an activated carbon based adsorbed natural gas storage system," *Industrial & engineering chemistry research*, vol. 50, no. 23, pp. 13 000–13 011, 2011.

[7] T. K. Bose, R. Chahine, and J.-M. St-Arnaud, "High-density adsorbent and method of producing same," Mar. 12 1991, uS Patent 4,999,330.

[8] J. F. Mengpin Ge, "4 charts explain greenhouse gas emissions by countries and sectors. retrieved march 23, 2020, from https://www.wri.org/blog/2020/02/greenhouse-gas-emissions-by-country-sector," Feb. 06 2020.

[9] H. Ritchie and M. Roser, "Co and greenhouse gas emissions. retrieved march 5, 2020, from https://ourworldindata.org/co2-and-other-greenhouse-gas-emissions," *Our World in Data*, 2017.

[10] K. Oura, V. Lifshits, A. Saranin, A. Zotov, and M. Katayama, *Surface science: an introduction*. Springer Science & Business Media, 2013.

[11] D. Hillel and J. L. Hatfield, *Encyclopedia of soils in the environment*. Elsevier Amsterdam, 2005, vol. 3.

[12] C. Erkey, "Thermodynamics and dynamics of adsorption of metal complexes on surfaces from supercritical solutions," *Supercritical Fluid Science and Technology Supercritical Fluids and Organometallic Compounds- From Recovery of Trace Metals to Synthesis of Nanostructured Materials*, pp. 41–77, 2011.

[13] M. Kajama, N. Nwogu, and E. Gobina, "Hydrogen permeation using nanostructured silica membranes," *Witpress*, vol. 193, pp. 447–456, 2015.

[14] S. Brunauer and P. H. Emmett, "The use of low temperature van der waals adsorption isotherms in determining the surface areas of various adsorbents," *Journal of the American Chemical Society*, vol. 59, no. 12, pp. 2682–2689, 1937.

[15] S. Brunauer, P. H. Emmett, and E. Teller, "Adsorption of gases in multimolecular layers," *Journal of the American chemical society*, vol. 60, no. 2, pp. 309–319, 1938.

[16] G. Cerofolini, L. Meda, and T. Bandosz, "Adsorption with soft adsorbents or adsorbates. theory and practice," in *Studies in Surface Science and Catalysis*. Elsevier, 1999, vol. 120, pp. 227–272.

[17] P. C. Hiemenz, *Principles of colloid and surface chemistry*. New York: M. Dekker., 1986, vol. 4.

[18] F. Ambroz, T. J. Macdonald, V. Martis, and I. P. Parkin, "Evaluation of the bet theory for the characterization of meso and microporous mofs," *Small Methods*, vol. 2, no. 11, p. 1800173, 2018.

[19] M. Thommes, K. Kaneko, A. V. Neimark, J. P. Olivier, F. Rodriguez-Reinoso, J. Rouquerol, and K. S. Sing, "Physisorption of gases, with special reference to the evaluation of surface area and pore size distribution (iupac technical report)," *Pure and Applied Chemistry*, vol. 87, no. 9-10, pp. 1051–1069, 2015.

[20] J. Rouquerol, F. Rouquerol, P. Llewellyn, G. Maurin, and K. S. Sing, *Adsorption by powders and porous solids: principles, methodology and applications*. Academic press, 2013.

[21] M. D. LeVan, *Fundamentals of adsorption: proceedings of the Fifth International Conference on Fundamentals of Adsorption*. Springer Science & Business Media, 2012, vol. 356.

[22] S. Qiu, G. Zhu, and Q. Fang, "Synthesis, structures and multifunctional properties of metal-organic open frameworks with intriguing molecular topologies," in *Studies in surface science and catalysis*. Elsevier, 2007, vol. 170, pp. 2004–2014.

[23] P. Horcajada, T. Chalati, C. Serre, B. Gillet, C. Sebrie, T. Baati, J. F. Eubank, D. Heurtaux, P. Clayette, C. Kreuz *et al.*, "Porous metal–organic-framework nanoscale carriers as a potential platform for drug delivery and imaging," *Nature materials*, vol. 9, no. 2, pp. 172–178, 2010.

[24] N. Fathma and Y.-K. Jeong, "Activities of metal-organic frameworks for the adsorption of clofibric acid from water," 2019.

[25] S. Hermes, F. Schröder, R. Chelmowski, C. Wöll, and R. A. Fischer, "Selective nucleation and growth of metal- organic open framework thin films on patterned cooh/cf3-terminated self-assembled monolayers on au (111)," *Journal of the American Chemical Society*, vol. 127, no. 40, pp. 13 744–13 745, 2005.

[26] S. Aguado, J. Canivet, and D. Farrusseng, "Facile shaping of an imidazolate-based mof on ceramic beads for adsorption and catalytic applications," *Chemical Communications*, vol. 46, no. 42, pp. 7999–8001, 2010.

[27] J. Liu, F. Sun, F. Zhang, Z. Wang, R. Zhang, C. Wang, and S. Qiu, "In situ growth of continuous thin metal–organic framework film for capacitive humidity sensing," *Journal of Materials Chemistry*, vol. 21, no. 11, pp. 3775–3778, 2011.

[28] H. Guo, G. Zhu, I. J. Hewitt, and S. Qiu, ""twin copper source" growth of metal- organic framework membrane: Cu3 (btc) 2 with high permeability and selectivity for recycling h2," *Journal of the American Chemical Society*, vol. 131, no. 5, pp. 1646–1647, 2009.

[29] O. Shekhah, H. Wang, S. Kowarik, F. Schreiber, M. Paulus, M. Tolan, C. Sternemann, F. Evers, D. Zacher, R. A. Fischer *et al.*, "Step-by-step route for the synthesis of metal- organic frameworks," *Journal of the American Chemical Society*, vol. 129, no. 49, pp. 15 118–15 119, 2007.

[30] S. Motoyama, R. Makiura, O. Sakata, and H. Kitagawa, "Highly crystalline nanofilm by layering of porphyrin metal- organic framework sheets," *Journal of the American Chemical Society*, vol. 133, no. 15, pp. 5640–5643, 2011.

[31] E. Biemmi, C. Scherb, and T. Bein, "Oriented growth of the metal organic framework cu3 (btc) 2 (h2o) 3 x h2o tunable with functionalized self-assembled monolayers," *Journal of the American Chemical Society*, vol. 129, no. 26, pp. 8054–8055, 2007.

[32] G. Decher, J. Hong, and J. Schmitt, "Buildup of ultrathin multilayer films by a self-assembly process: Iii. consecutively alternating adsorption of anionic and cationic polyelectrolytes on charged surfaces," *Thin solid films*, vol. 210, pp. 831–835, 1992.

[33] J. J. Richardson, M. Björnmalm, and F. Caruso, "Technology-driven layer-by-layer assembly of nanofilms," *Science*, vol. 348, no. 6233, p. aaa2491, 2015.

[34] H. V. Annapureddy, S. K. Nune, R. K. Motkuri, B. P. McGrail, and L. X. Dang, "A combined experimental and computational study on the stability of nanofluids containing metal organic frameworks," *The Journal of Physical Chemistry B*, vol. 119, no. 29, pp. 8992–8999, 2015.

[35] S. De, M. I. Nandasiri, H. T. Schaef, B. P. McGrail, S. K. Nune, and J. L. Lutkenhaus, "Water-based assembly of polymer–metal organic framework (mof) functional coatings," *Advanced Materials Interfaces*, vol. 4, no. 2, p. 1600905, 2017.

[36] O. I. Lebedev, F. Millange, C. Serre, G. Van Tendeloo, and G. Férey, "First direct imaging of giant pores of the metalorganic framework mil-101," *Chemistry of Materials*, vol. 17, no. 26, pp. 6525–6527, 2005, retrieved march 30, 2020. [Online]. Available: https://doi.org/10.1021/cm051870o

[37] H. Sun, "Compass: an ab initio force-field optimized for condensed-phase applications overview with details on alkane and benzene compounds," *The Journal of Physical Chemistry B*, vol. 102, no. 38, pp. 7338–7364, 1998.

[38] R. M. Stephenson, *Handbook of the thermodynamics of organic compounds*. Springer Science & Business Media, 2012.

[39] C.-X. Yang and X.-P. Yan, "Metal–organic framework mil-101 (cr) for high-performance liquid chromatographic separation of substituted aromatics," *Analytical chemistry*, vol. 83, no. 18, pp. 7144–7150, 2011.

PUBLICATIONS

PUBLICATIONS

List of Publications

- **3D Printing of Biomimetically Inspired Zircon for Ceramic Mold Components**
  P.P. Raikar, **T.C. Dube**, A. Tiamiyu, A.D. Ekwealor, A.S. Panuganti, C.C. Shorey, H.Y. Park, J. Zhang, Y.G. Jung
  POWDERMET/AMPM 2019, Phoenix, AZ , USA; June 2019
- **Optimization of Printing Parameters for 3D Printed PLA**
  N.H. Hawaldar, P.P. Raikar, **T.C. Dube**, J. Zhang
  MS&T Conference, Columbus, OH, USA; October 2018

Presentations

- **Injection Molding of NdFeB Magnets using 3D Printed Molds**
  T. C. Dube, H.Y. Park, Y.G. Jung, C. Macris, J. Zhang
  MIM 2020, Irvine, CA, March 2020
- **3D Printing of Biomimetically Inspired Zircon for Ceramic Mold Components**
  P.P. Raikar, **T.C. Dube**, A. Tiamiyu, A.D. Ekwealor, A.S. Panuganti, C.C. Shorey, H.Y. Park, J. Zhang, Y.G. Jung
  POWDERMET/AMPM 2019, Phoenix, AZ, June 2019
- **OptimizationOptimization of Printing Parameters for 3D Printed PLA**
  N.H. Hawaldar, P.P. Raikar, **T.C. Dube**, J. Zhang
  MS&T Conference, Columbus, OH, USA; October 2018

Posters

- **Developing 3D printed molds for injection molding of neodymium magnets**

  T.C. Dube, H.H. Choi, Y.G. Jung, J. Zhang

  2nd Annual ASM Indianapolis Chapter Spring Conference, Lafayette, IN, USA; February 2020

- **Experimental and Computational Modeling of Metal Organic Framework and Zeolite Coatings for Gas Adsorption and Emission Control**

  T. C. Dube, N.H. Hawaldar, P.P.Raikar, B.G. Kim, H. H. Choi, Y. G. Jung, J. Zhang

  Indiana Summit 2019, Indianapolis, IN; October 2019

- **Experimental and Modeling Study of Gas Adsorption of Gas Molecule in Metal Organic Framework and Zeolite**

  T. C. Dube, N.H. Hawaldar, P.P. Raikar, B.G. Kim, H. H. Choi, Y. G. Jung, J. Zhang

  POWDERMET/AMPM 2019, Phoenix, AZ; June 2019

- **Metal Organic Framework and Zeolite Coatings for Emission Control**

  T. C. Dube, N.H. Hawaldar, J. Zhang

  IUPUI Research Day 2019, Indianapolis, IN; April 2019

- **Experimental and Modeling Study of Gas Adsorption of Gas Molecule in Metal Organic Framework and Zeolite**

  T. C. Dube, N. H. Hawaldar, P. P. Raikar, B. G. Kim, H. H. Choi, Y. G. Jung, J. Zhang

  ASM Indianapolis Chapter Spring Conference, Columbus, IN, February 2019

Awards

- Metal Injection Molding Association (MIMA) student grant for Metal Injection Molding (MIM) conference 2020, Irvine, CA, USA, March 2020
- Metal Powder Industries Federation (MPIF) student grant for Powder Metallurgy/Additive Manufacturing with Powder Metallurgy (POWDERMET/AMPM) conference 2019, Phoenix, AZ, USA, June 2019